Nanoscale

REVIEW

View Article Online
View Journal | View Issue

Cite this: *Nanoscale*, 2023, **15**, 9256

Advances in functional organic material-based interfacial engineering on metal anodes for rechargeable secondary batteries†

Ruijuan Shi, *‡ Zhen Shen,‡ Qianqian Yue and Yong Zhao *

Metal anodes with the merits of high theoretical capacity and low electrochemical potential are promising candidates for the construction of high-energy-density rechargeable secondary batteries. However, metal anodes with high chemical reactivity are likely to react with traditional liquid electrolytes, leading to the growth of dendrites, side reactions, and even safety issues. In this case, metal plating/stripping electrochemistry is associated with an enhanced ion transfer rate and homogeneous ion distribution on the metal surface. Herein, functional organic material (FOM)-based interfacial engineering on metal anodes is systematically presented, focusing on the effects of forming uniform solid electrolyte interphase (SEI) layer, homogenizing ion flux, accelerating ion transport, *etc*. This main content addresses the advances of FOMs in terms of SEI modification, 3D skeleton construction, and gel/solid-state electrolytes in multiple metal batteries, providing in-depth insights into the exploration of high-performance metal batteries. Moreover, other applications and outlooks for FOMs are further summarized, paying potential ways for the practical applications of FOM-based rechargeable secondary batteries.

Received 21st March 2023,
Accepted 22nd April 2023

DOI: 10.1039/d3nr01306e

rsc.li/nanoscale

1. Introduction

In the last few decades, the global energy crisis and environmental problems have become urgent. As an important backup energy storage device, secondary batteries enable the further development of clean energy, reducing the consumption of fossil fuels and alleviating the deterioration of the environment.[1–3] In the development of high-energy-density devices, alkali (such as Li, Na, and K) and alkaline earth (*i.e.*,

School of Materials, Key Lab for Special Functional Materials of Ministry of Education, Henan University, Jinming Avenue, Kaifeng, 475001, P. R. China. E-mail: 10330121@henu.edu.cn, zhaoyong@henu.edu.cn

†Celebrating the 25th anniversary of the Key Laboratory for Special Functional Materials of Ministry of Education at Henan University.

‡These authors equally contribute to this work.

Ruijuan Shi

Ruijuan Shi received her B.S. Degree from Henan Normal University, Xinxiang, China, in 2014, and PhD from Nankai University, Tianjin, China, in 2020. Currently, she is a Lecturer at Henan University. Her research interests are focused on the fabrication of advanced electrode materials and electrolyte modification for rechargeable metal batteries.

Yong Zhao

Yong Zhao received his PhD in Physical Chemistry from the Institute of Chemistry, Chinese Academy of Sciences in 2008 under the supervision of Prof. Lei Jiang. Subsequently, he was a Post-Doctoral Fellow with Prof. Kazuhito Hashimoto in Applied Chemistry at the University of Tokyo (2008–2015). He became a Full Professor at Henan University in 2016. His research focuses on the mechanism of electrocatalytic reactions and catalyst innovation in fuel cells and advanced materials for rechargeable batteries.

Zn, Mg, Al, and Ca) metal batteries with high capacity have become next-generation high-energy-density batteries.[4–6] For example, zinc metal batteries have developed rapidly in recent years due to their high theoretical specific capacity (820 mA h g^{-1}), low cost, and environmental friendliness. However, the growth of dendrites and side reactions on Zn anodes are inevitable in liquid electrolytes, and the Coulombic efficiency of Zn deposition/stripping behavior remains unsatisfactory.[7–9] Similarly, alkali metal anodes with high chemical reactivity are prone to generating side reactions with the electrolyte to form an unstable solid electrolyte interphase (SEI) layer on the metal surface, resulting in the loss of active material, unstable SEI, uncontrollable dendrite growth, and severe volume expansion.[10,11] All these issues hinder the commercialization of rechargeable metal batteries, and thus there is an urgent requirement to explore dendrite-free, safe and highly stable rechargeable metal batteries.[12]

Generally, the unstable SEI layer is closely related to the slow ion transfer and uneven ion flux on the metal surface, and thus investigating schemes to suppress metal dendrite growth and side reactions is crucial for the construction of high-safety and high-energy-density energy storage devices. There are four main methods used, as follows: firstly, the construction of a three-dimensional (3D) skeleton, which can effectively promote the ion transfer rate, reduce the local current density, and enhance the uniform deposition of metals.[13] Secondly, the modification of the electrolyte. The electrolyte additives contribute to the *in situ* formation of an even SEI layer on the metal surface, which will improve the stability of the anode/electrolyte interface and reduce side reactions.[14–16] Thirdly, designing an artificial SEI layer. The introduction of artificial SEI layer can effectively avoid the direct contact between the liquid electrolyte and metal anode, reducing the loss of active substances and electrolyte.[17–19] Finally, the construction of gel/solid-state electrolytes (SSEs). This method inhibits dendrite growth and reduces side reactions, further improving the battery safety.[20–22] Among them, the modification of the SEI generally has a high ion transport rate and mechanical strength to induce uniform ion deposition, which also effectively inhibits the growth of dendrites and side reactions.[23] Besides, this method can be effectively combined with other strategies to construct rechargeable secondary batteries with high safety and high cycle stability.

The structural stability of the SEI layer determines the cycle life of metal anodes, and thus various strategies have explored to stabilize the SEI layer, such as regulating the electrolyte components and designing 3D skeleton structures.[24–26] Notably, the modification of the SEI with functional organic materials (FOMs) has attracted increasing attention due the abundant resources, structural designability, and eco-friendly nature of FOMs.[27] A favorable SEI layer with FOMs can prevent the excessive depletion of the electrolyte, limit the growth of dendrites, and minimize the volume change, while still allowing fast ion transport.[28,29] The reported FOMs for metal/electrolyte interface engineering mainly include small organic molecules, polymers, metal–organic frameworks (MOFs), covalent organic frameworks (COFs), metal-covalent organic frameworks (MCOFs), and other 2D materials.[30,31] The interfacial engineering of the SEI layer on metal anodes has witnessed great improvement with the addition of FOMs, owing to their effects of forming a uniform SEI layer, homogenizing the ion flux, accelerating ion transport, *etc*.[32,33] For example, small organic molecules in FOMs have flexible structures and small mass, which play an important role as electrolyte additives in stabilizing metal anodes.[34–37] Polymers with designable structures (such as polyvinylidene fluoride (PVDF), poly (ethylene oxide) (PEO), and polyvinyl alcohol (PVA)) usually take part in the construction of artificial SEI layers in the liquid electrolytes, as well as porous 2D COF and MOF materials.[28,38,39] Moreover, 2D materials with adjustable functions and designable structures can also be used as a 3D skeleton and solid/quasi-solid electrolytes, in combination with flexible polymers.[40–43] However, a polymer-based artificial SEI layer can mitigate dendritic growth and volume changes, but its high crystallinity leads to a low ion migration efficiency.[44,45] Besides, the practical application of COFs and MOFs with poor flexibility and crystallinity in SSEs or artificial SEI layers is limited by their low ionic conductivity and poor mechanical strength.[33,46,47] Therefore, a comprehensive review of the development and advances of FOM-based interfacial engineering is necessary, which will open up avenues toward the further exploration of high-performance rechargeable batteries.

FOM-modified anodes are mostly employed in the construction of high-performance alkali metal batteries, and their application in practical areas is foreseeable.[48] However, few reviews have systematically summarized the research on the use of FOMs in structural engineering for anode protection, and the metal deposition behaviors on FOMs are still lacking in-depth reviews.[27,33] Herein, the recent progress on the use of FOMs in secondary batteries is outlined. Various FOMs and their applications in different rechargeable metal batteries are summarized in detail, including electrolyte additives and SEI construction in anode protection, 3D skeleton construction, and solid/quasi-solid electrolyte. In this review, we summarize the use of FOMs in Li, Na, K, and Zn secondary batteries in recent years, emphasizing the advances and corresponding design strategies in liquid electrolytes and SSEs. The conclusion and outlooks for FOMs on the structural engineering of metal anodes are further discussed, paving potential ways for the practical application of FOM-based rechargeable secondary batteries.

2. Issues of current metal anodes

Although secondary batteries, particularly lithium metal batteries are being widely studied, their further development is hampered by several problems, including unstable SEI, dendritic growth, side reactions, volume change, and safety issues.[49–51] Thus, researchers have proposed numerous methods to alleviate these problems *via* the protection of metal anodes, improving the cycling stability of metal batteries. These strategies can be summarized into four aspects (Fig. 1), as follows: (1) design of artificial SEI layer, (2) regulation of the electrolyte, (3) construction of a 3D skeleton and

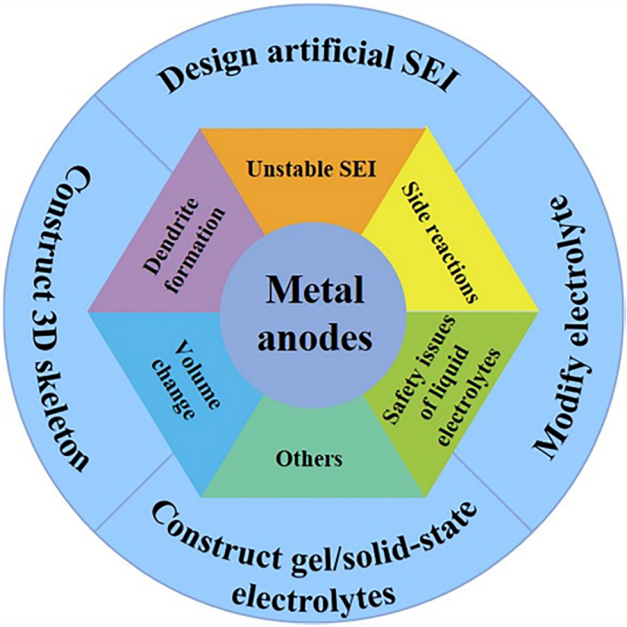

Fig. 1 Schematic diagram of the problems and common strategies of metal anodes.

(4) construction of gel/solid-state electrolytes.[13,21,34] These issues confronted by metal anodes are discussed below.

2.1. Unstable SEI film

Alkali and alkaline earth metals are a class of metals with a lower electrochemical potential, which means they are more reductive. Thus, they will react with the organic electrolyte to generate a large number of inorganic salts and organic salts, which cover the metal surface, forming a layer of electronic insulation SEI film.[10,52] However, the SEI layer generated *in situ* has the disadvantages of heterogeneous composition, loose morphology, and poor mechanical properties, owing to the slow ion transfer and uneven distribution of ion flux on the metal surface.[23] The unstable SEI cannot withstand the stress caused by the metal deposition and volume change. Consequently, a large amount of the liquid electrolyte and active metal are consumed, and the repeated damage and repair of the SEI will lead to the uneven local deposition on the metal surface, resulting in the production of dendrites and "dead lithium (sodium, potassium)".[53] The unstable SEI film not only increases the internal resistance of the full battery, but also reduces the Coulombic efficiency of the battery, leading to rapid battery failure and even safety hazard.[54] Therefore, modification to achieve a uniform and dense SEI is needed to protect the metal electrodes, preventing direct contact and side reactions between the electrolyte and the alkali and alkaline earth metals.

2.2. Side reactions

Alkali/alkaline-earth metal anodes with high chemical reactivity can spontaneously and irreversibly react with most of the electrolyte components. The side reaction can cause irreversible consumption of the active metal and electrolyte, leading to a low Coulombic efficiency and limited cycle life of batteries.[55,56] Simultaneously, the side reaction process will also produce a large amount of flammable gas, resulting in battery swelling, performance deterioration, and even great safety hazard.[21] For Zn metal batteries, hydrogen evolution is the most serious side reaction, which forms a passivation layer and affects the Zn^{2+} transport rate.[57] The gas pressure generated by the hydrogen evolution reaction will also gradually increase the volume of the battery and even burst the battery. Accordingly, electrolyte additives and artificial SEI films should be considered to prevent the continuous side reactions.

2.3. Dendrite formation

Dendrite growth can be attributed to the uneven ion deposition on the metal surface, owing to the uneven metal surface, mass transfer rate of electrolyte at different locations on the electrode surface, *etc.*[58] Dendrite growth risks penetrating the separator, resulting in direct contact between the positive and negative electrodes and triggering a short circuit. Furthermore, the formation of dendrites increases the surface area of the metal anode, leading to the irreversible consumption of the metal and electrolyte, which increases the polarization, gas production and other side reactions on metal anodes.[14,59] Due to dissolution and adhesion factors, some dendrites are easy to break away from the matrix surface during the cycle, which is the primary reason for capacity attenuation in metal batteries. Thus, the combination of SEI modification and 3D skeleton construction should be carried out to suppress the formation of dendrites.

2.4. Volume change

Metal without fixed substrate is repeatedly deposited and stripped on the anode during the charge and discharge cycle, resulting in large volume expansion at the anode. In addition, the continuous side reactions between the electrolyte and the metal can cause the collapse of the internal structure of the metal electrode. During this process, the metals in the SEI dissolve in the electrolyte, creating holes in the electrode. The large volume change stress causes the unstable SEI layer to fracture, and the electrolyte seeps into the electrode and further reacts with the alkali metal until the fresh metal or electrolyte is completely consumed. In addition, electrode pulverization causes dendrite fracture to generate "dead lithium (sodium and potassium)", which increases the internal resistance of the battery and hinders the transmission of ions in the battery. Thus, the construction of a 3D skeleton with an artificial SEI layer is an ideal way to alleviate the volume expansion of metal anodes.

2.5. Safety issues of liquid electrolytes

The traditional organic liquid electrolytes usually consist of flammable organic solvents and corrosive electrolyte salts, which are easy to react on the surface of the cathode material in the high oxidation state to produce flammable gas, resulting in electrical corrosion and damage. Besides, metal dendrites are easily formed on the anode surface, which will pierce the

separator and cause internal short circuit of the battery. Additionally, metal batteries with liquid electrolytes easily burn when subjected to severe impact, limiting the application of liquid batteries. In contrast, SSEs and non-flammable electrolytes have been proposed to improve the safety of rechargeable batteries, avoiding volume changes and the use of a large amount of liquid electrolyte.[60,61]

In conclusion, it should be noted that the above-mentioned issues are all related. An unstable SEI will cause side reactions and dendrite growth, which will make the metal anode volume expand, and then cause a series of safety problems. Dendrite growth and side reactions promote each other, consume a large amount of electrolyte and metal active substances during the cycle, continuously damage the anode, and lead to a decrease in the Coulombic efficiency of the electrode. Also, the volume expansion of the metal anodes will damage the SEI film and induce more serious side effects, resulting in a limited cycle life. Therefore, any methods that can regulate each of the above-mentioned aspects can greatly improve the electrochemical performance of metal batteries.

3. Types and functions of FOMs used in interfacial engineering

Most FOMs are easily accessible from natural raw materials and usually composed of light elements of C, H, O, B, N, S, *etc*.[62] The types of FOMs used in interfacial engineering can be mainly divided into small organic molecules, flexible polymers, COFs, MOFs, and other 2D materials (*e.g.*, MXenes, carbon nanotubes (CNTs), and graphene), as shown in Fig. 2.[27,63] The investigation on FOMs in rechargeable batteries

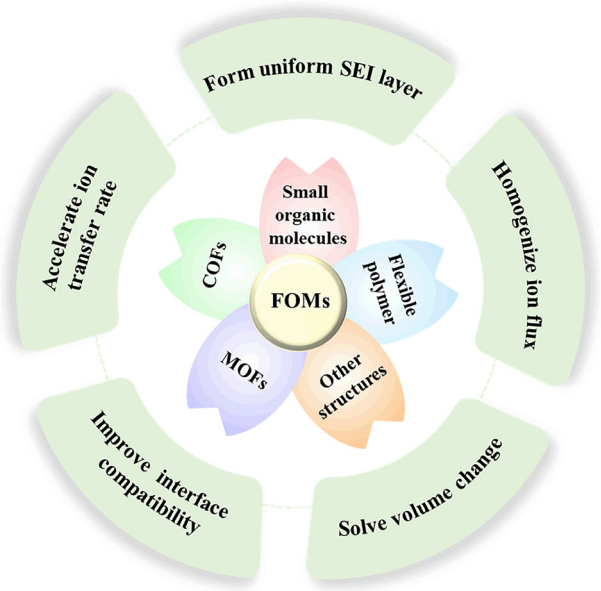

Fig. 2 Types and functions of FOMs used in interfacial engineering on metal anodes.

can be traced back to the advent of LIBs, as early as the organic electrolyte used in the Li primary battery in the 1960s. Small organic molecules in FOMs have flexible structures and small mass, which play an important role in stabilizing metal anodes as electrolyte additives.[64,65] Most ether (1,3-dioxolane (DOL), dimethoxyethane (DME), diglyme, *etc*.) and ester (propylene carbonate (PC), ethylene carbonate (EC), diethyl carbonate (DEC), dimethyl carbonate (DMC), *etc*.) solvents applied in organic electrolytes are typical small organic molecules of FOMs, and organic functional additives are also employed (fluoroethylene carbonate (FEC), thiourea, organic fluoride/phosphide, *etc*.).[66–68] The organic solvents used in the electrolytes have attracted increasing attention due to their merits of fast ion conductivity, good interface compatibility, structural diversity, and abundant resources. The FOM-based additives can promote the formation of high-performance *in situ* SEI due to their low cost, high efficiency, easy operation, and low impact on the electrolyte.[69–71] However, highly reactive metal anodes are likely to react with organic solvents containing functional groups, especially ester-based electrolytes, forming an original and uneven SEI on the metal surface.[72] The designed organic electrolytes with functional groups favor ion transport between the positive and negative electrodes, while the functional additives contribute to the formation of uniform SEI layers, resulting in enhanced Coulombic efficiency and cycling stability in rechargeable batteries.[73]

The unstable SEI layer always shows uneven ion flux and slow ion transfer rate, causing poor cycling stability and capacity fading in metal batteries. Polymers with designable structures (such as PVDF, PEO, polyacrylonitrile, poly(methyl acrylate) (PMA), and PVA) usually take part in the construction of artificial SEI layers in liquid electrolytes, owing to the advantages of the homogenized ion flux and fast ion transfer rate.[74–77] The enhanced mechanical strength of the artificial SEI can prevent the growth of metal dendrites, and uniform metal deposition helps to maintain the interfacial stability of metal anodes.[78–80] Moreover, considering their flexible structure and good interface compatibility, flexible polymers can be applied as SSEs to reduce voltage polarization.[81,82] Similarly, COFs and MOFs with porous structures and rigid channels are promising candidates for the formation of artificial SEI layers and gel/solid-state electrolytes, owing to their well-defined ion channels, enhanced mechanical strength, and homogenized ion deposition/stripping processes.[31,83,84] However, their poor flexibility cannot cope with the large volume changes during the battery cycling. In this case, COFs/MOFs with poor flexibility and processability can be improved by bottom-up structural design (grafted with flexible polymer chains or functionalized with acidic/anionic groups), combination with flexible polymers or 3D structures, and *in situ* formation on the metal surface. Besides, they are also used as 3D skeletons, separators and S-loading hosts, to accommodate the volume expansion of metal anodes, block the shuttle effect of the active materials, and increase the structural stability of S cathodes, respectively.[85–87] Nevertheless, the practical applications of COFs and MOFs in rechargeable batteries are limited by their

poor processability and complex synthesis process, which need further exploration and study with the support of advanced technological methods.[62,88]

Furthermore, FOMs with other 2D structures are widely used for the modification of the SEI, separators, and 3D skeletons.[89,90] In comparison to COFs, these 2D materials (*e.g.*, MXenes) exhibit less structural designability and higher electron conductivity, displaying high mechanical properties and abundant active group-grafted surface.[91] For example, MXenes with multiple grafted functional groups could improve the transport of Zn^{2+} effectively in combination with the polymer matrix.[92] Therefore, the design and study of 2D materials with grafted multifunctional surfaces for interfacial engineering should be highly desirable, offering new insights into the further exploration of high-performance rechargeable batteries (Table 1).

4. Advances in FOMs used as protection layers in secondary metal batteries

4.1. SEI modification in liquid electrolytes

SEI modification mainly includes electrolyte regulation and construction of artificial SEI films. Electrolyte regulation refers to the addition or changing a certain component in the electrolyte to form SEI *in situ* on the metal surface. The resulting *in situ* SEI layer has better contact with the metal interface, while the thickness and uniformity of the formed SEI are difficult to control.[101] The formation of an artificial SEI film involves the pretreatment of the metal before battery assembly, forming a uniform and dense passivation layer with a controllable thickness on the metal surface.[102] These two strategies to modify the SEI layer are widely used in secondary batteries, including Li, Na, K, Zn, Mg, and Al.

4.1.1. Lithium metal batteries. Lithium metal anodes with low redox potential and high theoretical capacity endow lithium metal batteries with high energy density.[103] However, lithium metal anodes face continuous dendrite growth and side reactions due to their unstable SEI layer and low Li^+ transport rate, resulting in short cycle life and low Coulombic efficiency. Peled *et al.* discovered that an SEI layer was formed on the Li surface when Li metal contacted with an organic electrolyte. This pristine SEI was not only an ionic conductor, but an electron insulator.[104] However, the self-formed SEI layer always showed poor cycling stability and homogeneity during the long deposition/stripping process. Based on the characteristics of organic materials, the SEI formed by organic materials has good mechanical strength and high Li^+ conductivity, which becomes an important component in the anode protection layer.

Table 1 The types and illustration of the structures of typical FOMs. Reproduced with permission.[93] Copyright 2022, Nature Publishing Group. Reproduced with permission.[94] Copyright 2019, Elsevier B.V. Reproduced with permission.[95,96] Copyright 2022, Wiley-VCH GmbH. Reproduced with permission.[97] Copyright 2019, The Royal Society of Chemistry. Reproduced with permission.[98–100] Copyright 2020 and 2022, the American Chemical Society

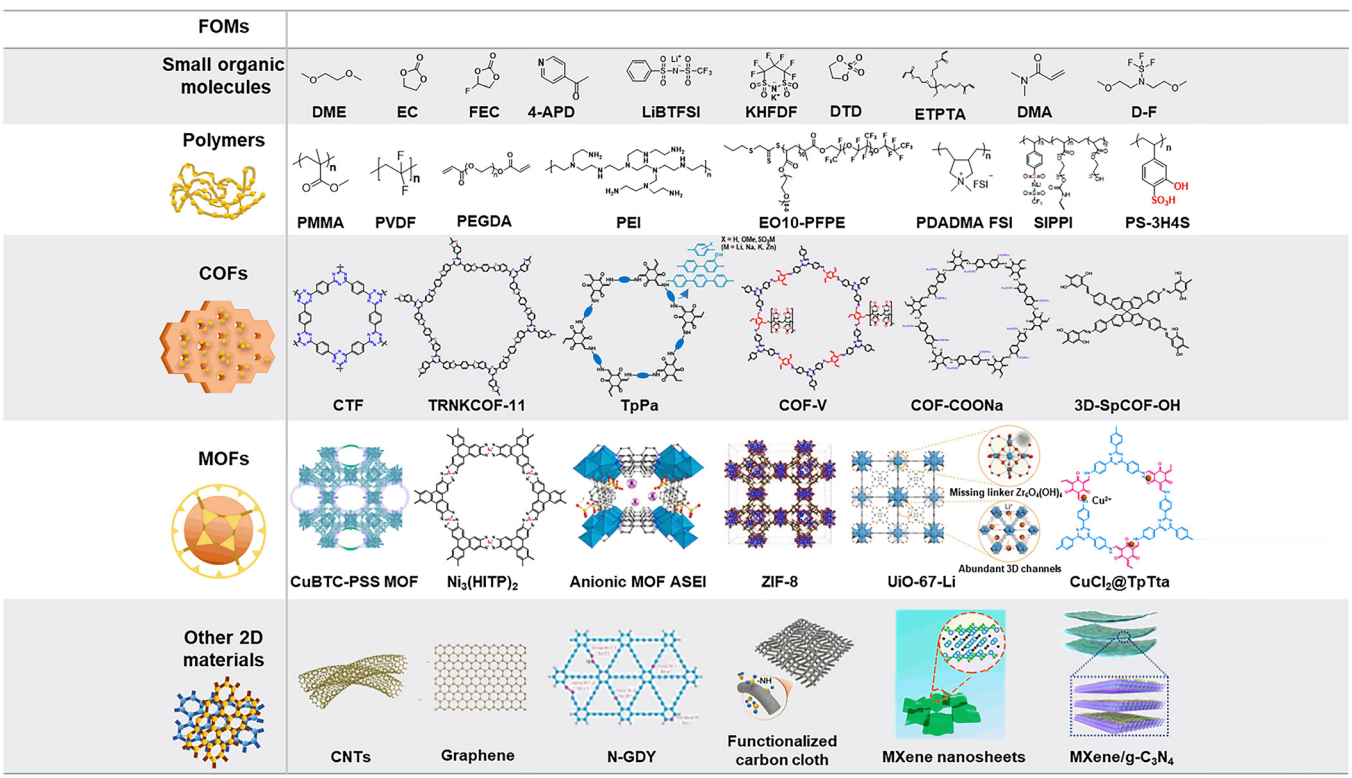

Given that the original SEI is prone to breakage during the repeated deposition/stripping process, organic materials are used as electrolyte additives to induce the formation of an artificial SEI or directly on the anode surface as a protective layer. For instance, Guo *et al.* induced the formation of an inorganic–organic composite SEI layer on the surface of a lithium electrode by using lithium difluorobis(oxalato) phosphate (LiDFOP) as an electrolyte additive (Fig. 3a), forming an $LiF/Li_xPO_yF_z$-rich inorganic SEI on the Li metal surface.[105] In addition, the cation-induced *in situ* ring-opening polymerization between LiDFOP and DOL contributed to the formation of a polymer organic SEI matrix. The Li||Li symmetrical batteries with a composite protective layer could achieve a cycle life of up to 1000 h at 1 mA cm^{-2} and a stable polarization voltage of 20 mV (Fig. 3b). Moreover, the LiDFOP-assembled Li||S batteries showed a discharge capacity of 910 mA h g^{-1} after 100 cycles (Fig. 3c). Unfortunately, the electrolyte additives are involved in the formation of the SEI layer, and thus their positive effect will diminish as they break down during the cycling process.

Moreover, the introduction of an artificial SEI layer in the alkali metal anodes before battery assembly is an effective strategy to protect the Li anode. In principle, the morphology of Li deposition largely depends on the structure of nucleation and the subsequent trend of nuclear growth, which is related to the surface energy and diffusion barrier.[106] Based on this, Zhao *et al.* prepared a functional film by coating perylene-3,4,9,10-tetracarboxydiimide organic molecules on the Li surface (PTCDI-Li), as shown in Fig. 3d. PTCDI-Li had lower diffusion barrier and higher surface energy than the bare Li metal, which could guide the homogeneous nucleation and growth of Li metal to achieve a dense morphology and dendrite-free lithium metal anode even at high current densities (Fig. 3e and f).[107] Therefore, high surface energy can generally promote multidimensional nucleation, and a low diffusion barrier is conducive to the uniform deposition of Li^+, which synergistically promote the uniform Li deposition in lithium metal batteries.

In general, the inner layer of the SEI formed by the decomposition of lithium salt in the electrolyte is mainly inorganic, and the outer layer is mainly an organic substance. Some researchers have reported that increasing the content of inorganic substances in the SEI is beneficial for improving its stability and mechanical strength. Based on this, Wang *et al.* synthesized two polymers, *i.e.*, C-1 (chain structure) and C-2 (crosslinked structure), to modify the surface of Cu foil and optimize the SEI composition (Fig. 4a).[108] Due to the interaction between the polymer and DOL solvent, the solvent consumption was reduced, while the decomposition of the Li salt was promoted, causing an increase in the content of LiF and Li_2S_x inorganic components in the SEI layer. Compared with the C-1 polymer, the SEI formed by the C-2 polymer had a

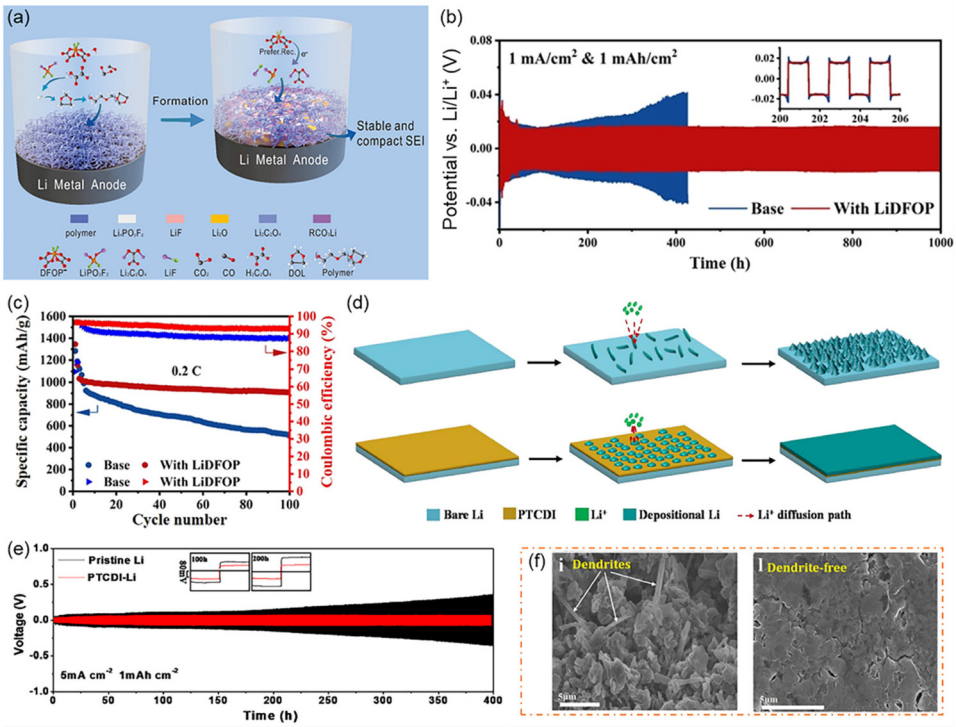

Fig. 3 (a) Schematic illustration of SEI generation induced by LiDFOP. (b) Charge/discharge curves of Li||Li symmetrical battery at 1 mA cm^{-2}. (c) Cycle performances of Li||S cells with/without LiDFOP additive at 0.2 C. Reproduced with permission.[105] Copyright 2021, the American Chemical Society. (d) Schematic diagram of deposition mechanisms of bare and PTCDI-protected Li anodes. (e) Cycling stability of Li||Li symmetrical cells with/without PTCDI-Li at 5 mA cm^{-2}. (f) SEM images of pure Li and PTCDI-Li after 120 cycles at 10 mA cm^{-2}. Reproduced with permission.[107] Copyright 2020, Elsevier B. V.

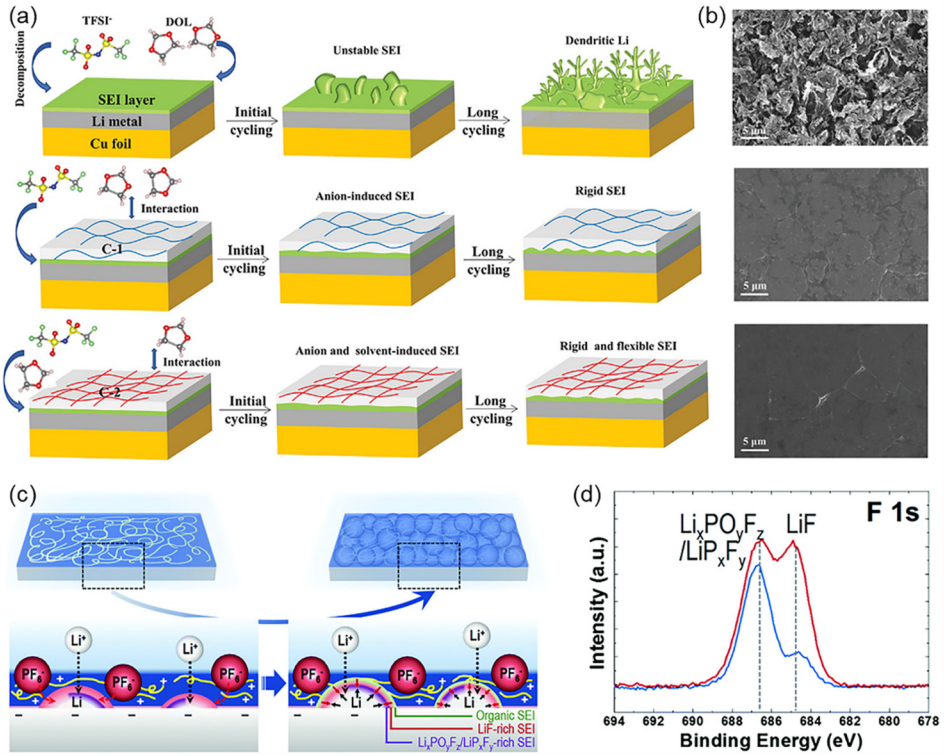

Fig. 4 (a) Schematic illustration of Li deposition behavior on different SEI layers. (b) SEM images of the surface of unmodified, C-1-modified, and C-2-modified Cu foils in Li||Cu batteries after 500 cycles at 0.2 mA cm^{-2}. Reproduced with permission.[108] Copyright 2022, Wiley-VCH GmbH. (c) Schematic diagram of electrochemical growth mechanism of Li metal with cationic PDDA polymer film. (d) High-resolution XPS F 1s spectrum on Cu foil without (blue) and with (red) cationic PDDA polymer films. Reproduced with permission.[109] Copyright 2020, The Royal Society of Chemistry.

moderate proportion of organic and inorganic components, showing a flatter deposition morphology (Fig. 4b) and enhanced cycling stability. Lee *et al.* reported a novel strategy for inhibiting dendrite growth with poly(diallyldimethylammonium chloride) (PDDA) cationic polymer, achieving LiF-rich SEI layers without providing additional fluorine in the electrolyte (Fig. 4c).[109] PDDA coating is an attractive cationic polymer electrolyte with high charge density, which could capture the PF_6^- in the electrolyte by electrostatic adsorption, forming an LiF-rich SEI layer with high ionic conductivity and chemical stability (Fig. 4d). This LiF-rich SEI layer facilitated the nucleation of lithium nanoparticles, inducing uniform Li stripping/plating behavior.

MOFs show great prospect in energy storage systems due to their modifiable functional groups and controllable morphology, which can effectively suppress the growth of Li dendrites by enhancing the mechanical strength and homogenizing the Li deposition/stripping processes.[110] Nevertheless, these strategies still cannot solve the problems of bulk metal lithium anode expansion and high interfacial impedance of unmodified SEI. Wu *et al.* designed an open-architecture MOF (OA-MOF) network (Fig. 5a), which could fully expose the lithiumphilic sites and promote interfacial charge transfer and uniform Li^+ flux, achieving even Li deposition morphology and smaller polarization voltage even at 3 mA cm^{-2}.[111] As shown in Fig. 5b, an Li||S full battery with an OA-MOF-based layer showed a discharge capacity of 815.5 mA h g^{-1} after 100 cycles. However, the main problem faced by the 2D-MOF layer is that the poor electrolyte infiltration hindered the transmission of Li^+, which may lead to higher polarization voltage and poor magnification performance.[112] Qian *et al.* synthesized nano-MOF-199 particles *via* a controlled simple liquid-phase reaction (Fig. 5c), which showed great potential in inhibiting dendrite growth and achieved an enhanced cycling performance and Coulombic efficiency (Fig. 5d).[113] The copper foil coated with MOF-199 had a uniform and dense porous shield layer, which could effectively reduce the loss of active lithium and the consumption of electrolytes, and also limit the growth of Li dendrites through the spatial effect.

COFs are porous crystalline polymers with high stability. COFs offer flexibility both in function and structure to effectively adjust the Li^+ migration and mechanical strength, thereby inhibiting lithium dendrite growth and side reactions.[114] Zhao *et al.* embedded LiF *in situ* in a COF material to obtain a new artificial SEI layer (Fig. 6a).[115] A β-ketoenamine-linked COF contributed to the trapping of high concentrations of Li salts in its abundant pores, resulting in the formation of anion-derived LiF-structured films in the original location of the COF (LiCOF-LiF). LiF particles were evenly dispersed in the COF matrix and closely combined with it, effectively preventing the penetration of the liquid electrolyte. Consequently, the LiCOF-LiF@Li||NCM full cells showed an improved cycle per-

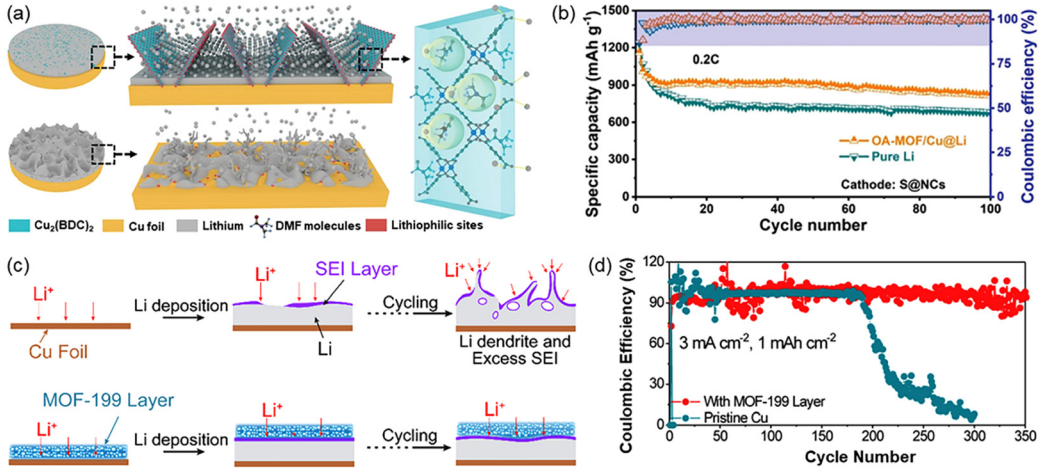

Fig. 5 (a) Schematic diagram of Li^+ flow and deposition on OA-MOF modified Cu surfaces with abundant lithiophilic sites and the planar Cu surfaces with few lithiophilic sites. (b) Comparison of cycle performance of pure Li and OA-MOF/Cu@Li anodes in Li||S batteries at 0.2 C. Reproduced with permission.[111] Copyright 2021, Wiley-VCH GmbH. (c) Schematic diagram of pristine and MoF-199-coated Cu electrodes during Li deposition/stripping process. (d) Coulombic efficiency of the blank and MOF-199-coated Cu electrodes at 3 mA cm^{-2} and 1 mA h cm^{-2}. Reproduced with permission.[113] Copyright 2019, Elsevier B.V.

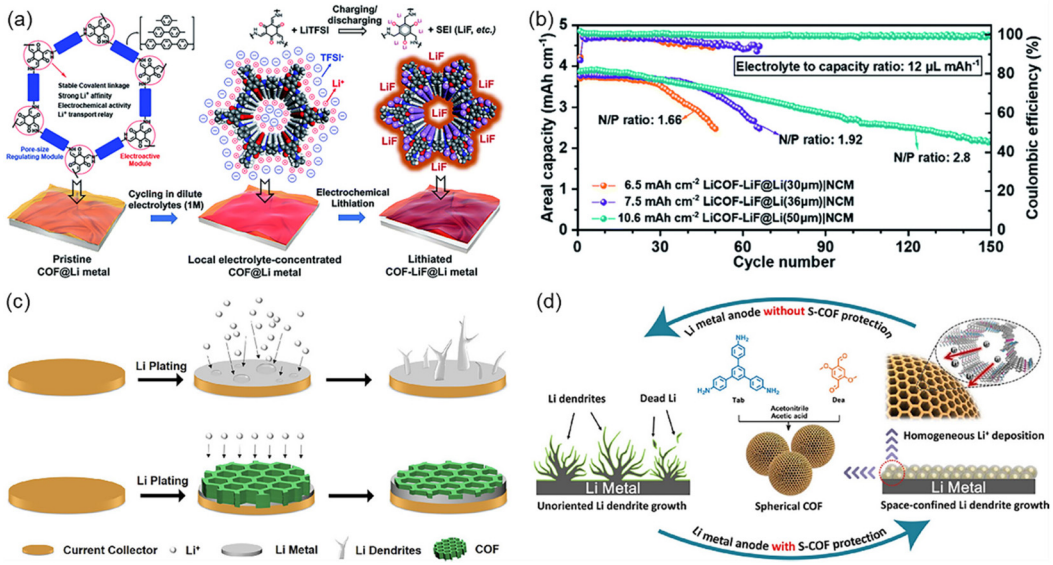

Fig. 6 (a) Illustration of the preparation process of COF-LiF interfacial layer on Li metal. (b) Cycle performance of LiCOF-LiF@Li||NCM with limited electrolyte and N/P ratio at 0.15 C. Reproduced with permission.[115] Copyright 2020, The Royal Society of Chemistry. (c) Schematic diagram of Li deposition behavior on bare and lithophilic COF-protected collectors. Reproduced with permission.[116] Copyright 2021, the American Chemical Society. (d) Schematic illustration of ion transport and deposition behaviors on the initial and S-COF-protected Li anodes. Reproduced with permission.[117] Copyright 2022, Elsevier B.V.

formance and high average Coulombic efficiency (over 99%) under harsh test conditions (Fig. 6b). Besides, Li *et al.* also synthesized a lithiophilic COF containing carbonyl groups and triazine rings (COF-TpTt) as a multifunctional SEI layer for lithium metal batteries (Fig. 6c).[116] In addition to carbonyl groups with Li^+ adsorption sites, the electron-rich triazine ring with lone pair could be used as a donor to attract Li^+. Consequently, the periodic arrangement of COF-TpTt guided the uniform distribution of Li^+ flux, ensuring the even and reversible deposition of Li metal with an ultralow polarization voltage (14 mV at 1 mA cm^{-2}).

In addition, Wang *et al.* successfully synthesized 3D spherical COFs (S-COFs), which could drive uniform Li^+ deposition using spatial confinement effects (Fig. 6d).[117] The polar lipophilic methoxy and imine bonds in the highly crystalline spherical COF structure further coordinated with Li^+, improving ion pair dissociation and unhindered Li^+ transfer process. S-COFs with ordered channels could efficiently distribute the

Li^+ flux uniformly under a low interfacial resistance, which could be owing to its accurate geometric symmetry and good morphology. However, it is difficult for organic polymers to possess mechanical strength and ionic conductivity simultaneously the because mechanical strength is closely related to the crystallinity of the polymer, while high ionic conductivity requires low crystallinity to migrate ion along the polymer chains.[118] Therefore, COFs with good mechanical strength and high ionic conductivity need further exploration to achieve dendrite-free and rapid deposition on Li anodes.

To improve the ionic conductivity of COFs, anionic and cationic groups are introduced on the skeleton of COFs, enhancing the electrostatic interactions between the functional groups in the versatile ionic COFs (ICOFs) and Li^+. In 2015, Du *et al.* reported the preparation of ICOFs, which showed good thermal stability and achieved high lithium ion conductivity at room temperature.[119] With the further research and exploration of ICOFs in recent years, Li *et al.* constructed a thin layer of anionic COF (ACOF) on the surface of a lithium anode to achieve favorable ion conduction and interface contact (Fig. 7a).[120] ACOF exhibited a microporous layered nanocrystal structure, and the anions filled around the framework could adsorb Li^+ and shield the anions to achieve rapid Li^+ conductivity. The layered structure caused the aromatic ring of ACOF to have a lower ion migration barrier, which indicated that Li^+ was more inclined to be uniformly distributed in the layered structure to achieve the dendrite-free dense deposition of lithium. Due to the synergistic effect of porous structure and functional groups, the ACOF-based protective layer on the surface of a lithium sheet could achieve a high ion mobility number (t_{Li^+} = 0.82) and an ionic conductivity of 3.7 mS cm^{-1} (Fig. 7b).

With further investigation, Zhang *et al.* used the bis(fluorosulfonyl)imide anion (FSI^-) as the coordination anion to construct a 2D ionic vinylene-connected COF (ivCOF-FSI) (Fig. 7c), which was equipped with a triazine ring for the easy desolvation of Li^+.[121] The ivCOF-FSI film could not only inhibit side reactions between the solvent molecules and active lithium but also accelerate the Li^+ transport in the SEI layer, thus forming a stable electrode/electrolyte interface. The ivCOF-FSI-protected Li||Cu half-cell could cycle for more than 390 cycles with a high average Coulombic efficiency of 99.2% (Fig. 7d). The ivCOF-FSI-protected Li anode delivered long-term Li deposition/stripping stability compared to the original Li electrode, and the bare Li anode showed fading Coulombic efficiency just after 71 cycles. This work opens a new avenue for the inter-

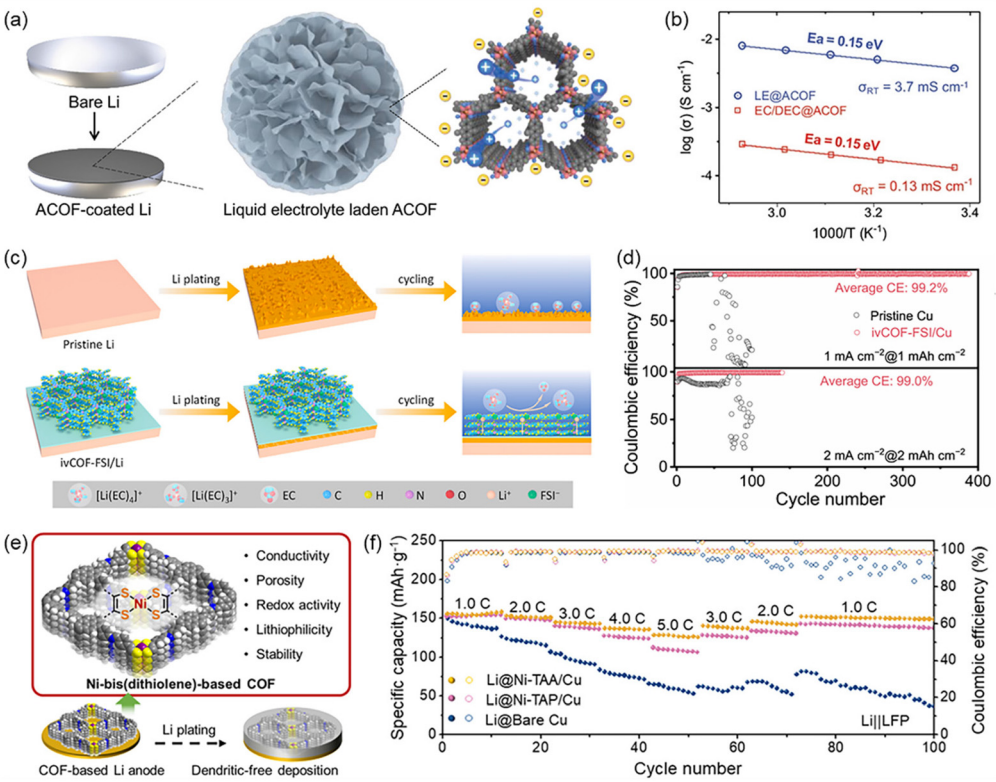

Fig. 7 (a) Schematic diagram of ACOF consisting of 2D nanoparticles. (b) Ionic conductivities of EC/DEC@ACOF and LE@ACOF electrolytes at various temperatures. Reproduced with permission.[120] Copyright 2021, Wiley-VCH GmbH. (c) Schematic illustration of Li^+ deposition behavior on the pristine Li and ivCOF-FSI/Li anodes. (d) Coulombic efficiency of bare Cu and ivCOF-FSI/Cu foils. Reproduced with permission.[121] Copyright 2022, Elsevier B.V. (e) Schematic diagram of structure of Ni-bis(dithiophene)-based COF and the Li deposition behavior on COF-based Li anode. (f) Rate performances of Li@Ni-TAA/Cu||LFP, Li@Ni-TAP/Cu||LFP, and Li@bare Cu||LFP full batteries. Reproduced with permission.[123] Copyright 2022, the American Chemical Society.

facial chemistry of solid–liquid interface on other alkali metal anodes.

The orientation of metal ions in porous COFs to form MCOFs may help to solve the problems of COFs of loose packing and surface compatibility.[122] By combining the advantages of MOFs and COFs, Ke *et al.* constructed two nickel-based MCOFs as protective layers (Fig. 7e), which showed excellent lithiophilicity and high ionic conductivity.[123] By introducing an Ni-bis(dithiolene)-based linker, the 4-connected tetra(aminophenyl)pyrene (TAP) or 3-connected tris (aminophenyl)amine (TAA) was connected to form Ni-TAP and Ni-TAA, respectively. The Ni-TAP and Ni-TAA assembled Li||Cu half-cell showed highly reversible Li deposition/stripping behavior, and the Coulombic efficiency of Ni-TAA/Cu maintained 99.1% after 220 cycles at 1 mA cm^{-2}. In addition, Li@Ni-TAA/Cu||LFP and Li@Ni-TAP/Cu||LFP full cells could provide appreciable discharge capacities of 140.3 and 122.3 mA h g^{-1} after 400 cycles at 1 C, respectively, and superior rate capability (Fig. 7f). Therefore, an artificial SEI layer with impressive lithiophilicity and ionic conductivity can effectively inhibit dendrite growth and achieve uniform Li deposition.

4.1.2. Sodium and potassium metal batteries. Sodium and potassium metal batteries with merits of low cost and abundant resources are promising alternatives to lithium metal batteries for large-scale energy storage systems, while the metals with high reaction activity are easily affected by the redox-active intermediates in the electrolyte, leading to poor cycling stability and low output capacity.[124] The existing methods to inhibit dendrite growth and side reactions mainly increase the Na^+/K^+ transport rate and mechanical strength and reduce the local current density of SEI films, thus improving the uniformity of sodium/potassium deposition and stripping.[25] The formation of a uniform and flexible SEI layer on the metal anode is an effective way to stabilize the anode/electrolyte interface and improve the cycling life of secondary metal batteries.

An increasing number of organic additives are added to the electrolyte to achieve an *in situ*/artificial SEI layer on the sodium anode, demonstrating the high ionic conductivity of the sodiophilic groups (such as NaF, Na–O, and Na_xS_n).[125,126] For instance, Forsyth *et al.* studied the effects of the NaFSI salt concentration and pretreated potential on the interface chemistry of sodium electrolyte using atomic force microscopy and molecular dynamics simulations, demonstrating the good cycling stability of the dendrite-free metal anode with a molten-salt-like structure.[127] Additionally, Wu and colleagues reported the use of an organosulfur compound additive (tetramethylthiuram disulfide, TMTD) as an interface protection layer to stabilize the sodium anode in carbonate-based electrolytes (Fig. 8a).[126] The stable stripping/plating cycling (more than 1600 h in Fig. 8b) of sodium metal batteries was enabled by the *in situ*-formed SEI with rich organic sulfide salts, as well for the full battery using Prussian Blue cathode (80% capacity retention after 600 cycles). To elucidate the underlying mechanism of the protective effect of SEI on an Na anode, Kong's research group monitored the formation process and chemical evolution of SEI derived from sodium difluoro(oxalato)borate (NaDFOB), as shown in Fig. 8c.[128] The protection effect offered by the borate/fluoride-rich SEI layer was tested in Na||Na symmetric cells with different pre-cycles, indicating the gradual evolution of the DFOB anion during cycling (Fig. 8d). Consequently, the $Na_3V_2O_2(PO_4)_2F$ (NVOPE)||Na full cell with borate/fluoride-rich SEI layer after 50 pre-cycles showed the longest life span, as shown in Fig. 8e (with a capacity retention of 94% after 2500 cycles).

Notably, Zhu *et al.* constructed a sodium benzenedithiolate (PhS_2Na_2)-rich protection layer *via* an *in situ* method to present the sodium dendrite growth in carbonate electrolyte (Fig. 9a and b).[71] The PhS_2Na_2 organic salt had a critical effect on the Na plating/stripping performance, leading to 800 h cycling life for dendrite-free sodium metal batteries (Fig. 9c). This result provides a promising strategy to suppress the growth of sodium dendrites *via* the use of organic sodium salts rather than traditional inorganic salts. Generally, polymers with multiple functional groups, mechanical strength, and flexible structure are suitable to effectively protect the high-reactive Na metal.[129] Archer and colleagues reported functional ionic polymer films on metallic sodium *via* the *in situ* electropolymerization of imidazolium-type ionic liquid (IL) monomers in liquid electrolytes (Fig. 9d).[130] The protected Na anodes exhibited a high Coulombic efficiency (as high as 95%) and stable long-term cycling (more than 120 cycles) at 1 mA cm^{-2}, as shown in Fig. 9e. Besides, Li's research group presented a free-standing PMMA/graphene film on Na metal surface to stabilize the Na anode upon repeated electrochemical stripping/plating, as shown in Fig. 9f.[131] The PMMA/graphene films with tunable thickness (Fig. 9g) on Na anode displayed a stable cycling performance for over 300 h at 2 mA cm^{-2}, providing in-depth insights into high-energy-density Li/Na metal batteries.

Moreover, an organic–inorganic (NaF-PVDF) hybrid protective layer was prepared on a Cu current collector *via* a direct coating method.[125] NaF in the hybrid protective layer could improve the Na^+ diffusion conductivity, and flexible PVDF could maintain the compatibility of the Na/coating interface, leading to an excellent cycle life of over 2100 h at 1 mA cm^{-2} and at 50% depth of discharge based on the hybrid protective layer. The uniformity of NaF particles could affect the Na^+ flux on the anode, while how to homogenize the distribution of sodiophilic sites is crucial to achieve a uniform and stable Na metal anode.

In contrast, the weak solvation of K and Na ions offers faster diffusion in electrolytes compared to Li ions.[132] Much effort has been devoted to exploring organic interface protection for potassium metal anodes, mainly by regulating the electrolyte composites and constructing 3D skeleton hosts.[133] According to Wu's work, it was firstly reported that the KFSI/DME electrolyte enabled reversible potassium plating/stripping behavior with high Coulombic efficiency (~99%), as shown in Fig. 10a, owing to the uniform SEI on the K surface.[134] This work contributes to a better understanding of the SEI layer and potassium plating/stripping electrochemistry (Fig. 10b), promoting the development of high-performance potassium metal battery technologies. Dai and colleagues reported the

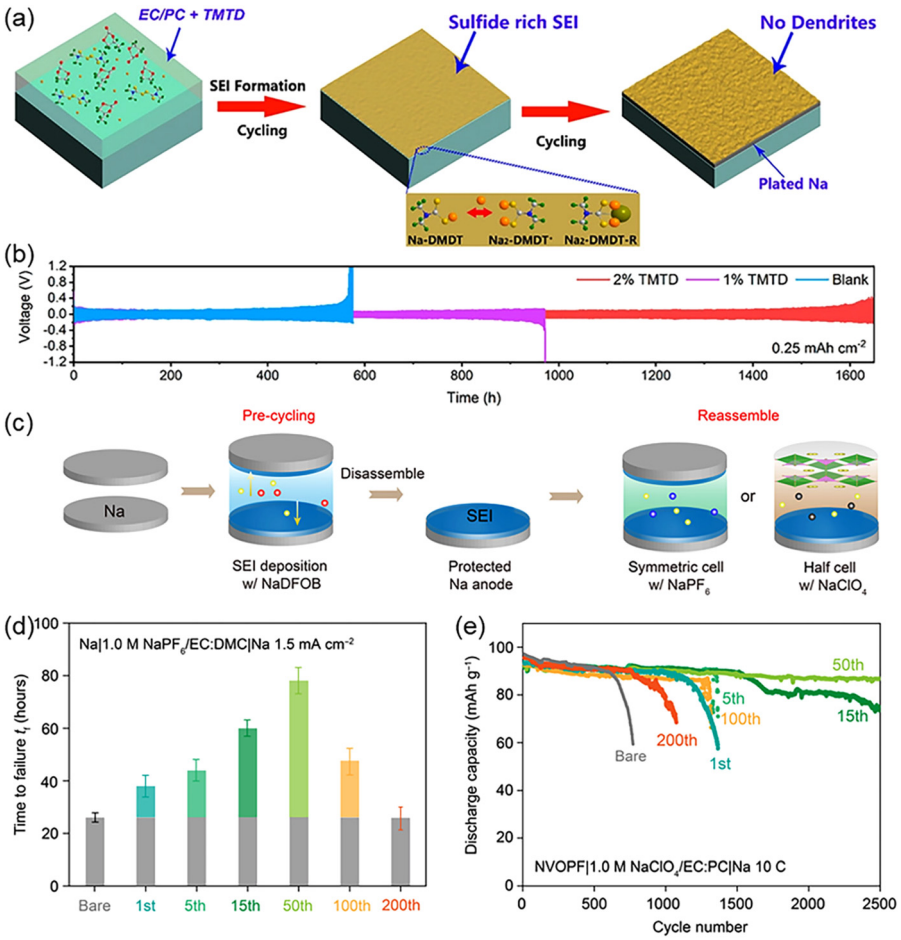

Fig. 8 (a) Schematic diagram of surface morphology of the treated sodium anode in TMTD-added electrolyte. (b) Cycling stability comparison of Na||Na symmetric cells in different electrolytes at 0.25 mA cm^{-2}. Reproduced with permission.[126] Copyright 2021, the American Chemical Society. (c) Schematic illustration of the SEI formation and reassembled workflow of protected Na anodes. (d) Time to failure of the reassembled Na||Na symmetric cells after different pre-cycles. (e) Cycling performance comparison of reassembled NVOPF||Na full cells with different pre-cycles of SEI coating. Reproduced with permission.[128] Copyright 2022, Lina Gao *et al.*

use of an intrinsically non-flammable IL electrolyte, combined with $AlCl_3$/KCl/KFSI, as the electrolyte in a high-safe potassium metal battery.[135] Particularly, robust K, Al, F, and Cl-containing passivating interphases are afforded both on the cathode and anode interfaces, leading to a high Coulombic efficiency of ~99.9% and excellent cycling stability (89% capacity retention after 820 cycles) for the potassium metal battery. Besides, Gu *et al.* constructed a uniform and elastic SEI *via* the *in situ* electro-polymerization (ISEP-SEI) of IL electrolytes.[132] The ISEP-SEI layer with excellent elasticity and uniformity could maintain the potassium metal with good interface integrity (Fig. 10c). Consequently, the K||K symmetric batteries with ISEP-SEI could cycle for 5000 h, and the ISEP-SEI-protected K||Prussian Blue full cell showed a stable cycle performance for 400 cycles at 0.5 A g^{-1} (Fig. 10d). Lu's group demonstrated that the cyclic anion of hexafluoropropane-1,3-disulfonimide-based electrolytes with highly efficient passivation ability was promising to mitigate the "dead K" and improve the cycling stability of high-voltage potassium-metal batteries, as shown in Fig. 10e.[136] The potassium-metal batteries with a high-voltage polyanion cathode (4.4 V) exhibited excellent cycling stability (Fig. 10f), enabling the fabrication of high-performance alkali metal batteries.

4.1.3. Zinc metal batteries. Although lithium metal batteries can partially address the issue of storing new energy, their widespread use is currently constrained by their flammable electrolyte, the limited supply of lithium, and safety risks.[137,138] As a result of these issues, a new generation of energy storage devices with high capacity, high safety, and affordable cost is being investigated by researchers, for example, zinc metal batteries with high energy density and cycle stability are one type of ideal candidates for large-scale energy storage devices.[139,140] Besides, Zn has many advantages, such as abundant natural reserves, low price and high specific energy, which will play a huge role in future energy storage systems.[141,142]

Aqueous electrolytes provide numerous potential merits over organic electrolytes, including low cost, easy operating

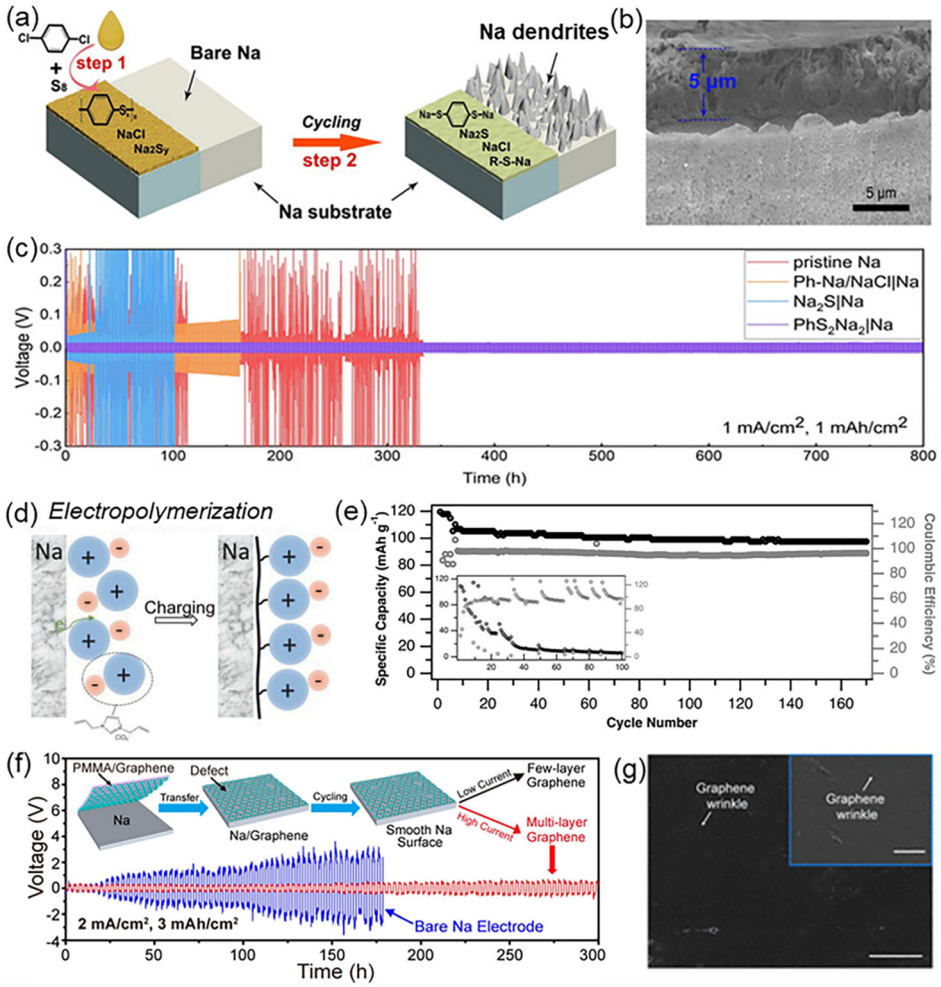

Fig. 9 (a) Schematic diagram of a PhS_2Na_2-rich protection layer on sodium metal surface. (b) SEM image of the protected layer on Na anode. (c) Long-term cycling performance of symmetric Na||Na cells with different types of electrodes. Reproduced with permission.[71] Copyright 2020, Wiley-VCH GmbH. (d) *In situ* formation of polymeric IL film on Na anode. (e) Electrochemical performance comparation of Na||$Na_3V_2(PO_4)_3$ (NVP) batteries with and without protected Na metal anode. Reproduced with permission.[130] Copyright 2017, Wiley-VCH GmbH. (f) Illustration of surface morphology and cycling stability of graphene-coated Na anode during the repeated electrochemical stripping and plating. (g) SEM image of ML-G/Na anode surface after 100 cycles. Reproduced with permission.[131] Copyright 2017, the American Chemical Society.

requirements, safety, and environmental friendliness.[143,144] However, the cycling performance of aqueous-based Zn metal batteries is damaged by the serious corrosion and dendrite growth.[145,146] Yu *et al.* designed a highly hydrophobic Zn_x-diethylenetriaminepenta (methx-phosphonic acid) (Zn_x-DTPMP) layer to provide Zn^{2+} attraction sites on the metal surface, achieving uniform and smooth Zn deposition (Fig. 11a).[147] The hydrophobic Zn_x-DTPMP layer reduced electrode corrosion and induced a uniform distribution of Zn^{2+} flux (Fig. 11b and c), causing the modified Zn symmetric battery to exhibit a cycle life of up to 1300 h at relatively low hysteresis voltages, as shown in Fig. 11d. Huang *et al.* found that the addition of γ-butyrolactone (GBL) could significantly improve the Zn electroplating/stripping performance.[148] GBL weakened the solvation between Zn^{2+} and H_2O, which rearranged the bonding network between particles and reduced the activity of water, inhibiting the formation of corrosion and byproducts (Fig. 11e). Besides, considering the unstable structure of the pristine protective layers, Yu *et al.* proposed the design of a methyltriethoxysilane-based protective layer with hydrophobic donor to prevent hydrogen evolution corrosion on the Zn anode.[149] Meanwhile, hydroxy ethylidene diphosphonic acid with a phosphate group was introduced in the SEI layer to form a strong chelating bond with Zn, which ensured the effective adhesion of the protection layer on the Zn anode. Consequently, the protected Zn symmetric cells exhibited a significantly long life of over 2000 h at 1 mA cm^{-2}, indicating the improved ion migration kinetics and uniform deposition of Zn^{2+} on the multifunctional layer-protected Zn anode.

Moreover, Kim *et al.* induced pyrrole oxidation polymerization (PPy) by reacting dilute HNO_3 with zinc metal to produce NO^+, and the hydrogen generation contributed to the *in situ* formation of 3D nanostructures (Fig. 12a).[150] The 3D-PPy could not only regulate the volume changes and Zn dendrite

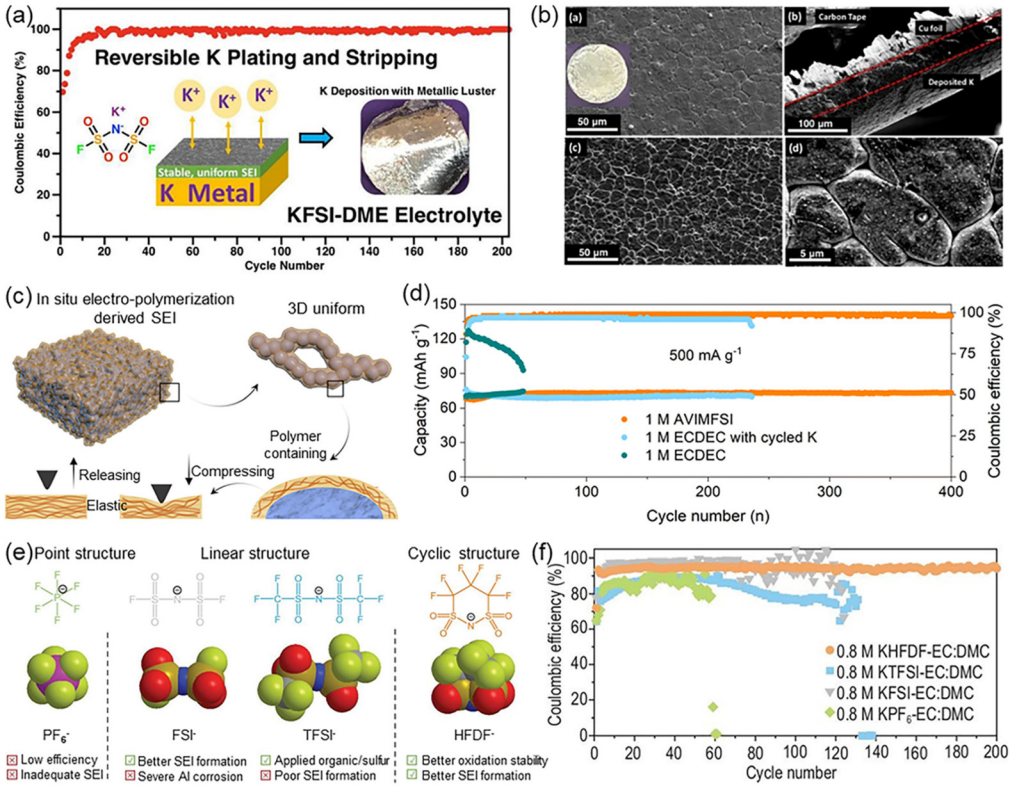

Fig. 10 (a) K plating and stripping performance on the Cu substrate at the rate of 0.05 mA cm^{-2}. (b) SEM images of the electrochemically plated K (3 mA h) in 0.1 M KFSI/DME electrolyte (K deposition at 0.05 mA cm^{-2} and 0.5 mA cm^{-2} corresponds to the right images, respectively). Reproduced with permission.[134] Copyright 2017, the American Chemical Society. (c) Schematic illustration of the structure and elasticity of the *in situ*-formed ISEP-SEI. (d) Comparison of the cycle performance of K||Prussian Blue cells in different electrolytes at 0.5 A g^{-1}. Reproduced with permission.[132] Copyright 2023, The Royal Society of Chemistry. (e) Design concept and molecular structure of the anions in this work. (f) Cycling performance of K||Cu half-cells in different electrolytes. Reproduced with permission.[136] Copyright 2022, China Science Publishing & Media Ltd.

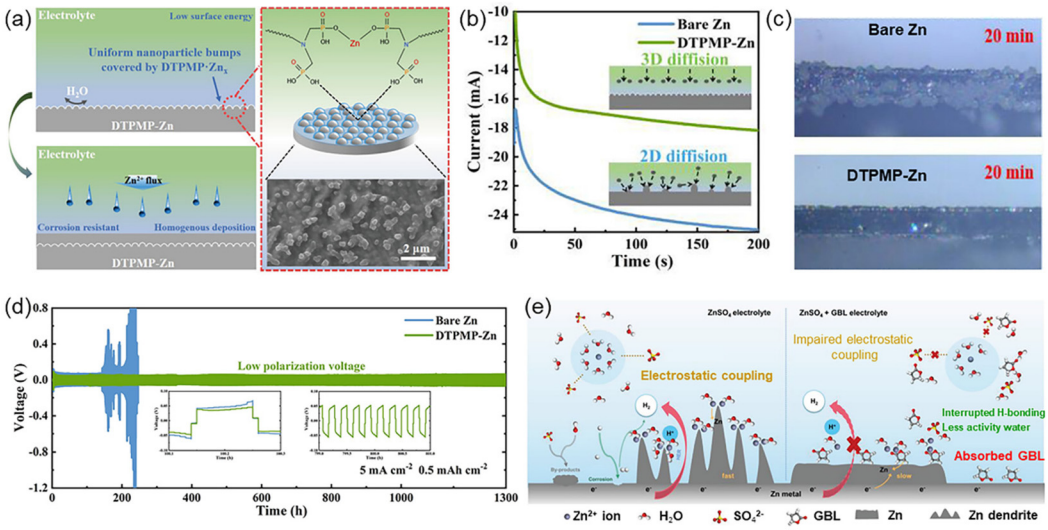

Fig. 11 (a) Schematic image of Zn deposition behavior on DTPMP-Zn anode. (b) Chronoamperometry curves of bare and DTPMP-coated Zn anodes at the overpotential of –150 mV. (c) Optical microscopy images of bare Zn and DTPMP-Zn anodes after plating for 20 min at 10 mA cm^{-2}. (d) Long-term cycling performance of bare and DTPMP-coated Zn||Zn symmetric cells under the condition of 5 mA cm^{-2} and 0.5 mA h cm^{-2}. Reproduced with permission.[147] Copyright 2022, the American Chemical Society. (e) Schematic illustration of Zn deposition behaviors in $ZnSO_4$ and $ZnSO_4$-GBL electrolytes. Reproduced with permission.[148] Copyright 2022, Wiley-VCH GmbH.

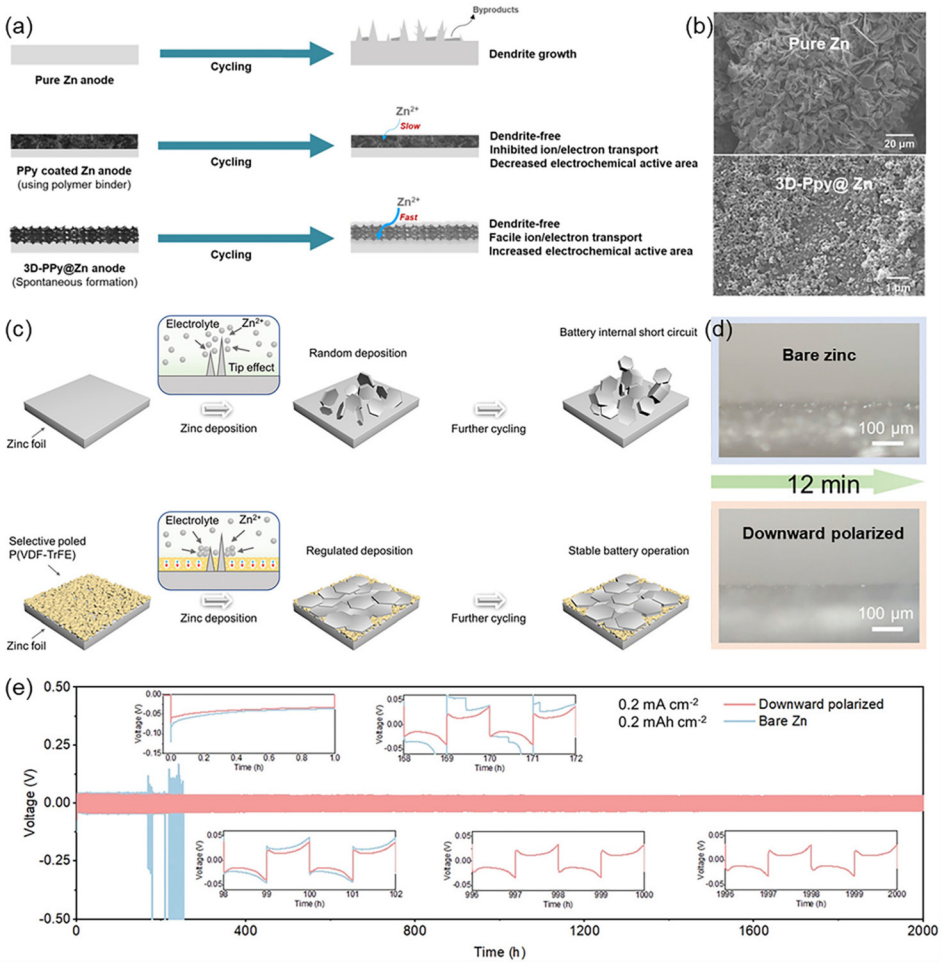

Fig. 12 (a) Schematic illustration of Zn deposition on the pure Zn, PPy-coated Zn, and 3D-PPy@Zn anodes. (b) SEM images of bare Zn (top) and 3D-PPy@Zn anodes (bottom) after cycling for 300 h and 1500 h, respectively. Reproduced with permission.[150] Copyright 2022, Elsevier B.V. (c) Schematic profiles of Zn deposition behaviors on the surface of bare Zn (top) and P(VDF-TrFE)-coated Zn (bottom) anodes. (d) *In situ* optical microscopy images of Zn plating behaviors on bare (top) and P(VDF-TrFE)-coated (bottom) Zn foils. (e) Cycling stability of symmetric Zn||Zn batteries with bare and coated Zn anodes. The insets show parts of the enlarged charge/discharge curves. Reproduced with permission.[151] Copyright 2022, Wiley-VCH GmbH.

growth process through mechanical protection, but also bring abundant electrochemical active sites to facilitate ion transport (Fig. 12b). Therefore, the assembled symmetric cells exhibited a long-term Zn deposition/stripping process for up to 1500 h at 1 mA cm^{-2}. Wang *et al.* developed a rigid poly(vinylidene fluoride-trifluoroethylene (P(VDF-TrFE)) coating to guide zinc growth rather than inhibit it, owing to the 90% crystallization and the stiffness of P(VDF-TrFE) increased significantly after heating.[151] After polarizing the polymer substrate with a controlled external electric field from the downward direction, an internal electrostatic field could be generated to induce localized concentrated Zn^{2+} on the surface of the coated polymer and achieve the uniform deposition morphology of Zn metal (Fig. 12c and d). In addition, P(VDF-TrFE) with a small amount of zinc trifluoromethanesulfonate ($Zn(OTf)_2$) nanoparticles could form a randomly distributed porous morphology in the polymer coating, which provided sufficient channels for Zn metal growth and Zn^{2+} diffusion.

Similarly, Cao *et al.* separated the drainage electrolyte from Zn by coating the surface of zinc metal with a hydrophobic zinc-salt modified MOF layer (Fig. 13a).[152] The modified MOF layer with 3D channel structure could restrict the hydrophobic $Zn(TFSI)_2$-tris(2,2,2-trifluoroethyl)phosphate (TFEP) organic electrolyte and form a ZnF_2-$Zn_3(PO_4)_2$ SEI layer on Zn anode, which could further prevent the trace H_2O dissolved in the organic electrolyte of $Zn(TSI)_2$-TFEP layer and reduce H_2O corrosion and side reactions of the Zn anode (Fig. 13b). More interestingly, the ZnF_2-$Zn_3(PO_4)_2$ SEI also had self-healing capabilities, and the $Zn(TFSI)_2$-TFEP-protected Zn anodes achieved 99.9% Coulombic efficiency and dendrite-free Zn deposition. Unlike alkali metals, an SEI could not be formed at the zinc metal anode and aqueous electrolyte interface, and the poor infiltration between the electrolyte/anode interface may lead to high voltage polarization. Liu *et al.* constructed an MOF composite protective layer to improve the poor infiltration of aqueous electrolyte in the Zn anode, as shown in

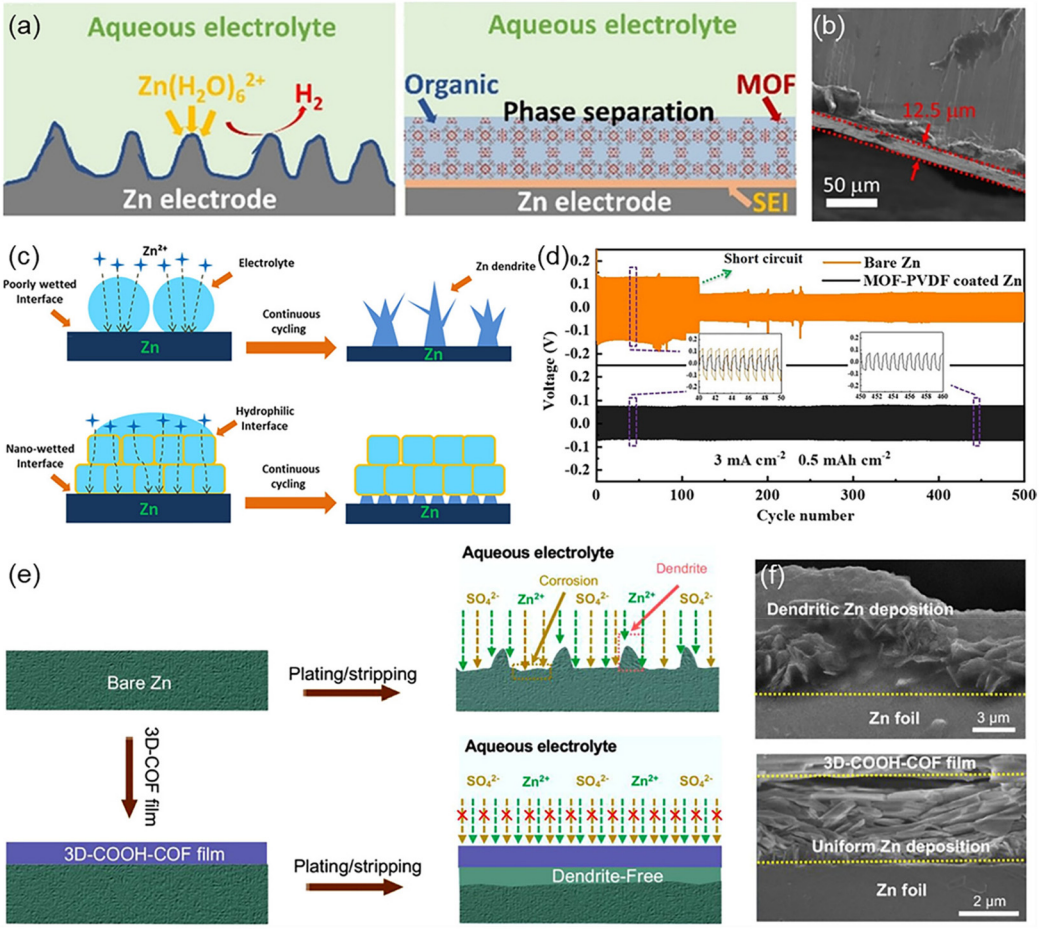

Fig. 13 (a) Schematic illustration of metal surface bare (right) and MOF-modified (left) Zn anodes. (b) SEM image of the deposition/striping of Zn metal in $Zn(TFSI)_2$-TFEP@MOF/H_2O electrolyte after 100 cycles at 0.5 mA cm^{-2}. Reproduced with permission.[152] Copyright 2020, Wiley-VCH GmbH. (c) Illustration of Zn deposition behaviors on bare and MOF-PVDF-protected Zn anodes during continuous cycling. (d) Galvanostatic charge/discharge curves of Zn||Zn symmetric cells using different Zn anodes at 3 mA cm^{-2}. Reproduced with permission.[153] Copyright 2019, the American Chemical Society. (e) Schematic profile of Zn deposition process on bare and 3D-COOH-COF-modified Zn anodes. (f) Cross-sectional SEM images of blank and 3D-COOH-COF-modified Zn anodes at 1 mA cm^{-2}. Reproduced with permission.[155] Copyright 2022, Elsevier B.V.

Fig. 13c.[153] By coating Zn anodes with PVDF and MOFs with chemically inert and microporous structures, the MOF-PVDF interface showed better wettability and lower interfacial charge transfer resistance compared to bare Zn. The good interfacial wettability maximized the solid–liquid contact and further promoted the Zn^{2+} transport flux, which reduced the overpotential of the Zn||MnO_2 cells during long-term cycling at high rates (Fig. 13d).

The merits of permanent porosity, ordered structure and adjustable skeleton of COFs have attracted increasing attention to protect Zn anodes. Hu *et al.* prepared zinc electrodes using a 2D high-crystallinity alkynyl-based COF (COF-H) as an artificial protective layer.[154] Due to the large number of electron-rich sites (acetylene, keto and enylamine) in COF-H, Zn^{2+} could be evenly distributed in 2D COF-H, which inhibited the formation of zinc dendrites and increased the corrosion resistance of Zn metal surface. Wu *et al.* synthesized a homogeneous and dense 3D-COOH-COF protective layer with hydrophilic functional groups and microporous morphology (Fig. 13e), which offered good hydrophilicity and high ionic conductivity to reduce the generation of dendrites and the interface impedance (Fig. 13f).[155] Meanwhile, the 3D-COOH-COF film exhibited good adhesion on the surface of the Zn anode, and the Zn||Zn symmetric batteries exhibited stable cycling for over 2000 h at 1 mA cm^{-2}.

4.1.4. Magnesium/aluminum metal batteries. Magnesium/aluminum metal batteries are promising alternatives in large-scale energy storage systems owing to their abundant reserves, high specific capacity, good safety, *etc.*[156,157] Unlike the lithium oxides and salts with accessible ionic conductivity, SEI layers containing magnesium salts usually display poor Mg^{2+} diffusion capability and irreversible stripping/plating behavior. In the case of Al metal, the aluminum oxide/hydroxide passive film on the surface of Al is thermodynamically irreversible in aqueous electrolytes, accompanied with self-corrosion and parasitic hydrogen evolution.[158] ILs are always applied to alle-

viate the self-corrosion of Al metal, as well as the structural modification of Al anodes.[159] Therefore, the exploration of reversible Mg/Al electrochemistry is crucial to realize the practical application of magnesium/aluminum metal batteries.[160,161] Generally, the potential electrolytes for Mg metal batteries include Grignard-based, boron-based, and IL electrolytes. For example, various fluoride alkyl magnesium salts with high solubility and interfacial compatibility were introduced in Mg metal batteries, which favored the *in situ* formation of a robust SEI layer on the Mg anode. The perfluoro-*tert*-butanol magnesium-based electrolyte enabled the Mg||Mg asymmetric cell to exhibit an ultralong cycling performance for over 2000 h and a Coulombic efficiency of 99.5%.[162]

The early artificial interphase layer on Mg metal surface was constructed from thermal-cyclized polyacrylonitrile and Mg trifluoromethanesulfonate, which could promote the reversible deposition/stripping process of the Mg anode.[163] The elastic and Mg^{2+}-conductive polymeric interphase prevented the direct contact between Mg metal and carbonate-based electrolyte, endowing the polymeric SEI-protected Mg/V_2O_5 full cell with reversible cycling performance (over 1000 h) and fast diffusion of Mg^{2+}. Similarly, Zhao *et al.* reported the preparation of an artificial SEI layer comprised of N-rich organic compounds and halide salts, which was derived from an aluminum chloride-1-ethyl-3-methylidazolium chloride IL.[164] The aluminum electrochemical cells with artificial IL-based SEI layer showed excellent reversibility and high specific energy (~500 W h kg^{-1} in Al||MnO_2 cell based on MnO_2 mass). Notably, the surface coating with high ionic conductivity could block the serious self-corrosion and insulating passivation of the Mg metal, which could facilitate Mg^{2+} transport and uniform Mg deposition.[165] Recently, Zhang *et al.* constructed a defect-free MOF membrane on Mg surface, which was designed to realize selective Mg^{2+} transport and uniform deposition of Mg metal.[166] The MOF/Mg electrodes with IL incorporated in the MOF showed improved interfacial charge transfer kinetics (with an exchange current of 6.3×10^{-4} mA cm^{-2}) and long-term stability (with a polar voltage of 0.75 V over 100 h). In contrast, the cell voltage of bare Mg electrode increased to 2 V within 5 h, indicating the high migration barrier of the passive layer on pristine Mg metal. This work provides a new idea to regulate the ionic transport pathways of porous MOF-based SEI layers in rechargeable metal batteries.

4.2. Constructing 3D skeleton

2D porous materials (MOFs/COFs) with the combined properties of stable skeleton, well-defined pore channels, and low density provide desirable lithium hosts for Li^+ transport/separation, which can reduce the current density of electrodes, uniformize the electric field distribution, and relieve volume changes.[167,167] Zhu *et al.* demonstrated that lithiophilic carbonized metal–organic frameworks (Li-cMOFs) with abundant Zn clusters and 3D conductive porous structure enabled the homogenization of the distribution of Li nucleation sites and Li^+ flux (Fig. 14a–c).[168] Similarly, Zhao and colleagues introduced $Ni_3(HITP)_2$ films on Cu foil as a current collector, as shown in Fig. 14d.[169] The lithiophilicity of MOFs can reduce the initial nucleation overpotential, and the Li||Li symmetrical cell with $Ni_3(HITP)_2$@Cu foil exhibited a high Coulombic efficiency of 99.7% after 900 cycles (Fig. 14e). Nevertheless, COFs cannot hybridize well with the insoluble 2D nanosheets to get stable COF-based nanohybrids, which could decay the ionic/charge transfer efficiency during the lithium storage process. In particular, Guo *et al.* reported the preparation of a 2D COF-on-MXene heterostructure with covalent assembly process (Fig. 14f), which was used as a suitable host for dendrite-free and fast-charging lithium anode.[170] The accessible lithiated COF channels and conductive MXene endowed fast Li^+ transport and ultralow Li nucleation/deposition overpotential (Fig. 14g and h). The covalent assembly of COFs on 2D conductive materials extends the applications of MXene-based heterostructures, which affords resultant nanohybrids with effective mass/charge transfer as anode hosts.

Similarly, the freestanding MXene/carbon nanotube scaffold with modified groups could be used to confine Na/K metals. The sodium/potassium-philic MXene sheets contribute to reduce local current density and homogeneous Na^+/K^+ flux on the MXene skeleton, enabling high electronic/ionic transport and enhanced stability during the Na/K plating/stripping processes. Cao *et al.* synthesized an MXene-coated carbon cloth ($Ti_3C_2T_x$-CC) host with highly metallic conductive and multiple sodiophilic sites for a flexible sodium metal anode (Fig. 15a).[100] The $Ti_3C_2T_x$-CC host efficiently induced the initial nucleation and oriented deposition of Na metal, avoiding the formation of mossy/dendritic Na metal. Consequently, the Na-$Ti_3C_2T_x$-CC electrodes derived from thermal infusion treatment presented high cycling stability and stripping/plating capacity, providing a strategy for the MXene-based protection of flexible Na metal anode (Fig. 15b and c). Similarly, Wang and colleagues reported the preparation of a titanium-deficient *N*-containing MXene/carbon nanotube (DN-MXene/CNT) freestanding scaffold for confining potassium metal, which exhibited a dendrite-free morphology and high efficiency (improved to ≈98.6% over 200 cycles) for high-performance potassium metal batteries (Fig. 15d).[171] The nucleation guidance from the DN-MXene sheets contributed to a uniform potassium distribution in the scaffold upon cycling (Fig. 15e and f). Besides, the full batteries with the K@DN-MXene/CNT anode and sulfur-poly(acrylonitrile) (SPAN) cathode showed a better rate performance in comparison to the bare K||SPAN full cells (Fig. 15g), which provides a novel way to enhance the potassium plating/stripping electrochemistry in stable potassium metal batteries. In addition, Mai's group designed practical carbon-based composite anodes by infiltrating molten potassium during the amine functionalization of the carbon scaffolds.[99] The highly potassiophilic amine groups accelerated the compatibility of the anode/electrolyte interface, providing abundant nucleation sites and nondendritic morphology for potassium metal anodes.

The emerging Na–K liquid alloy with deformation and self-healing properties shows high capacity, no dendrites, and

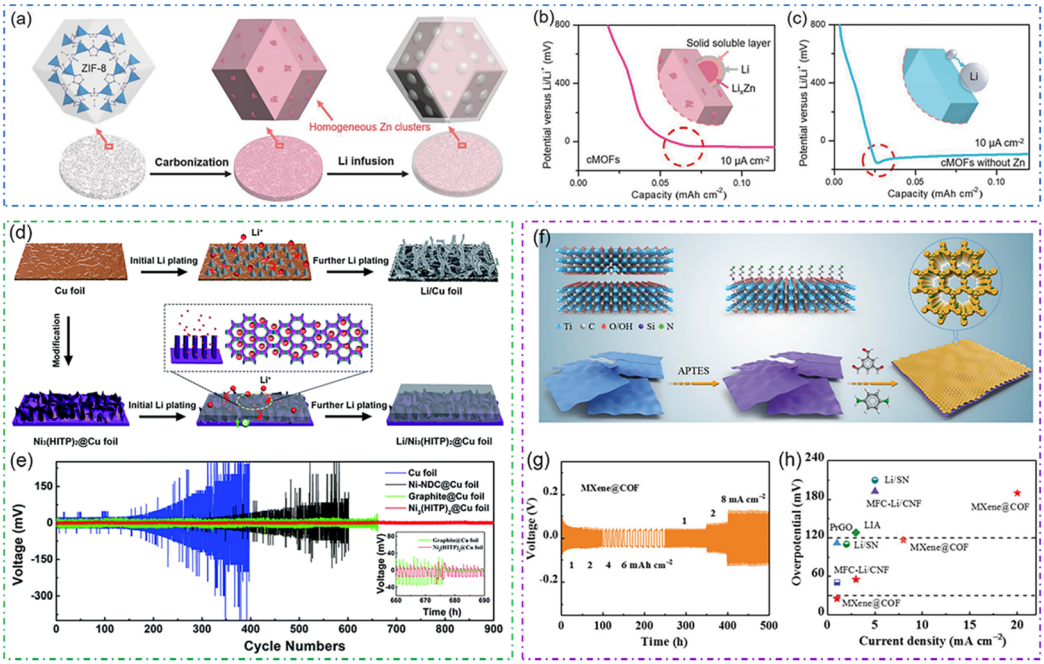

Fig. 14 (a) Illustration of the preparation of Li-cMOFs *via* a molten lithium infusion approach. Comparison of nucleation overpotential of Li deposition on carbonized ZIF-8 (b) with or (c) without Zn clusters. Reproduced with permission.[168] Copyright 2018, Wiley-VCH GmbH. (d) Schematic illustration of Li plating process on $Ni_3(HITP)_2$@Cu foil or Cu foil. (e) Cycling performance of Li symmetrical cells with different current collectors. Reproduced with permission.[169] Copyright 2021, The Royal Society of Chemistry. (f) Illustration of the fabrication of 2D MXene@COF heterostructure by the MXene covalent amination method. (g) Cycling performance of MXene@COF/Li symmetrical cell at different current densities. (h) Voltage hysteresis comparison of MXene@COF/Li anode with other reported 3D-host-based lithium anodes. Reproduced with permission.[170] Copyright 2021, Wiley-VCH GmbH.

slight volume change during the Na/K plating/stripping processes, which is regarded as ideal alternative for Na/K metal anodes. However, the practical electrochemistry of the Na–K alloy anode is limited by its high surface tension and fluidity, while infiltrating liquid Na–K alloy in the electronic conductive matrix is commonly applied as an efficient immobilization approach to achieve a dendrite-free stripping/deposition performance. For example, an Na–K alloy electrode coupled with an *in situ*-formed graphite intercalation compound network enabled the fabrication of stable alkali metal alloy batteries (Fig. 16a).[172] The Na–K composite electrode exhibited ultrahigh cycling stability without dendrite growth (maintaining the stable electrodeposition over 5000 h at 20 mA cm^{-2}), owing to the enhanced Na/K deposition nucleation on the conductive framework and the self-healing behavior of the Na–K liquid alloy (Fig. 16b and c). To improve the compatibility between Na–K liquid alloy anode and electrolyte, Wang *et al.* treated the hydrazone linkages of covalent organic frameworks (Tf-DHzDM-COFs) with a reducing agent (Na–K alloy), achieving carbon–oxygen radical COFs for high-energy alkali metal batteries (Fig. 16d).[173] The COR-Tf-DHzDM-COFs@Na–K composite anode could not only effectively inhibit dendrite formation, but also exhibit excellent cycle stability of K and Na metal batteries (Fig. 16e and f), which was associated with the synergistic effect of fast electron/mass transport of the cross-linked networks and the self-healing feature of the Na–K alloy.

Furthermore, 3D substrates have obvious advantages in improving the growth of zinc dendrites. They can increase the surface area of the matrix, reduce the local current density, and control the migration of Zn^{2+}, thus maintaining the stability of the cell volume.[174] Zhou *et al.* synthesized a foldable aerogel (MGA) using a 3D MXene and graphene, and the highly zincophilic framework caused zinc to be densely packed in a 3D manner on the microscale, effectively alleviating dendrite growth.[41] In addition, the inherent fluorine terminal group of MXene could form a ZnF_2-rich SEI on the metal surface *in situ*, leading to a flat deposition morphology without dendrites and fast kinetics for MGA@Zn electrodes. The quasi-solid-state Zn metal battery assembled by the MGA@Zn anode provided an initial capacity of 110 mA h g^{-1} and a capacity retention of 90.3% under continuous folding at 2C. Therefore, the construction of a stable 3D framework is essential for the application of zinc metal batteries.

4.3. FOM-based gel/solid-state electrolytes

LIBs assembled with typical liquid electrolytes are faced with the uncontrollable growth of dendritic lithium and detrimental side reactions, as well as electrolyte leakage and safety issues.[175] Accordingly, SSEs have been proposed with the merits of stable electrochemical performance, wide electrochemical window, and enhanced thermal stability.[176–178] Currently, the SSEs can be divided into inorganic solid electrolytes and polymer solid electrolytes. Inorganic solid electro-

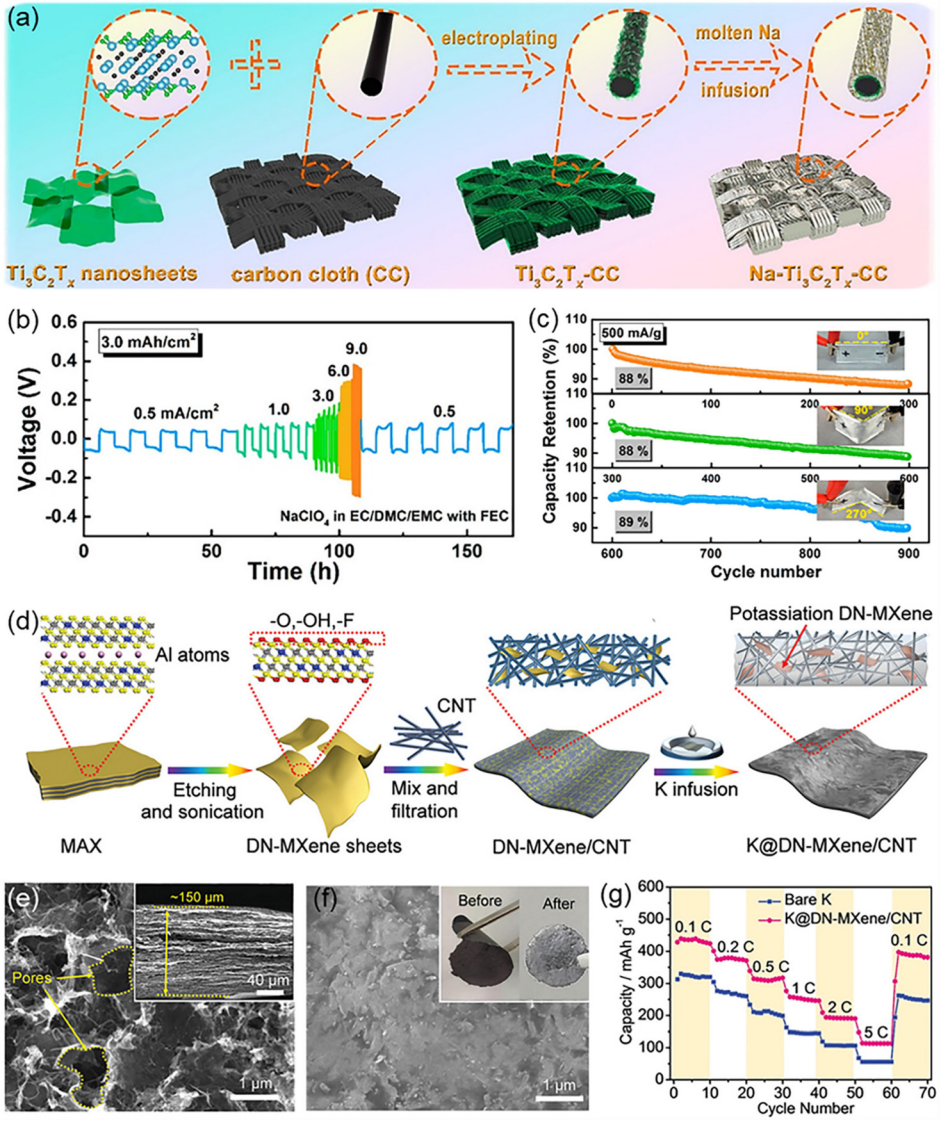

Fig. 15 (a) Schematic illustration of the fabrication process for Na-$Ti_3C_2T_x$-CC metal anode. (b) Rate performance of Na-$Ti_3C_2T_x$-CC at different current densities with a capacity of 3.0 mA h cm^{-2}. (c) Cycling stability of Na-$Ti_3C_2T_x$-CC||NVP cells under different bending angles. Reproduced with permission.[100] Copyright 2020, the American Chemical Society. (d) Schematic diagram of the preparation of K@DN-MXene/CNT metallic anodes. Top-view SEM images of (e) DN-MXene/CNT scaffold and (f) K@DN-MXene/CNT metallic anodes. (g) Rate capability comparation of K@DN-MXene/CNT||SPAN and bare K||SPAN K–S batteries. Reproduced with permission.[171] Copyright 2020, Wiley-VCH GmbH.

lytes have attracted wide attention due their high ionic conductivity and superior mechanical strength, while their practical application is limited by the poor interfacial wettability and inherent rigidness of inorganic compounds.[106,179] In contrast, polymer solid electrolytes show good interface compatibility, structural designability, and abundant raw materials.[180,181] However, their poor ionic conductivity and inferior mechanical strength are still urgent problems to be solved.[182,183] Nevertheless, the emerging polymer solid electrolytes with ionic conductivity or massive electrolyte salts offer SSEs a chance to approach practicality.[184,185]

For solid lithium metal batteries, Manthiram's group presented an electrolyte-mediated single-Li^+-conductive COF-based electrolyte, and the *in situ* solidification of liquid electrolyte could raise the charge-carrier concentration among SSEs (Fig. 17a–c).[186] The increased Li^+ conductivity in the DMA@LiTFSI-mediated COF (DLC) electrolyte was attributed to the release/decoupling of Li^+ ions from the rigid COF backbone with the help of functional groups of flexible DMA chains in the solid polymer electrolyte (SPE). Therefore, the DLC electrolyte with high flexibility exhibited a stable cycling performance for over 450 h (Fig. 17d), enabling the fabrication of a foldable SSE battery for practical applications. Besides, Hu and colleagues designed a topological polymeric solid electrolyte with 21 poly(2,2,2-trifluoroethyl methacrylate) fluoropolymer arms and postmodified β-CD core (21-β-CD-*g*-PTFEMA), as

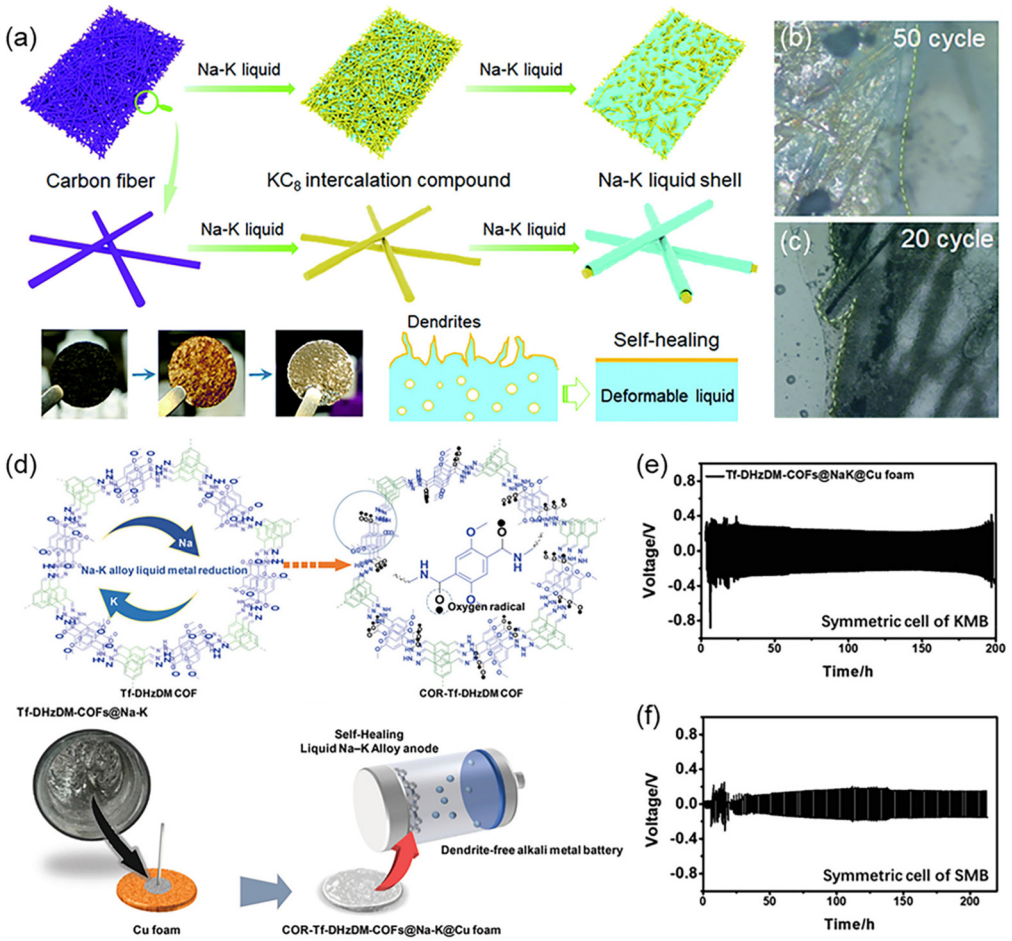

Fig. 16 (a) Schematic diagram of NaK-G-C electrode fabrication and preparation process. Optical microscopy images of the interface morphology of (b) NaK-G-C and (c) MK-G-C alloy anode at specific cycles of stripping/deposition. Reproduced with permission.[172] Copyright 2019, Elsevier B.V. (d) Schematic illustration of the synthesis and fabrication process of COR-Tf-DHzDM-COF@Na–K composite anode. Cycling stability of symmetric cells of COR-Tf-DHzDM-COF@Na-K@Cu foam in (e) potassium and (f) sodium metal anodes. Reproduced with permission.[173] Copyright 2022, Wiley-VCH GmbH.

shown in Fig. 17f.[187] The X-ray tomography and SEM images (Fig. 17g and h, respectively) showed that there were no Li dendrites with the use of FMC-ASPE-Li electrolyte, indicating uniform Li plating/stripping. Consequently, the LMFP|FMC-ASPE-Li|Li pouch cell showed a discharge capacity of ~2.47 mA h and stable cycling performance over 200 cycles (Fig. 17i).

The structural design of efficient ion conductive/transport pathways in SPEs has been a challenge for the development of all-solid-state batteries. COFs are an emerging class of crystalline polymer electrolytes with periodic structure and tunable functionality, while their ion conductivity is usually limited by their block structure and requires a certain amount of solvent support.[188] Horike and colleagues designed a flexible COF-based electrolyte with glassy PEO moieties through a bottom-up self-assembly approach, as shown in Fig. 18a.[83] The Li^+ conductivity was affected by the dynamics and length of the PEO chains in COF-based electrolyte (Fig. 18b), and the solid-state lithium battery using the as-synthesized COF-PEO-9-Li showed a discharge capacity of 120 mA h g^{-1} (Fig. 18c), suggesting the great potential of functional groups with dynamics on COF-based architecture in solid-state batteries. Moreover, Niu *et al.* introduced lithiophilic groups and quinolyl aromatic ring linkages in COFs applied as SSEs in lithium metal batteries, as shown in Fig. 18d.[189] The as-prepared quinolyl-linked COF (Q-COF) SSE thin films displayed an ion conductivity of 1.5×10^{-4} S cm^{-1} (Fig. 18e), owing to the holistically oriented channels in the Q-COF SSE film *via* the crystallographic orientation. The Li|Q-COF SSE|Li symmetrical cells showed stable cycling stability over 1000 h and low polarization voltage (about 50 mV) at 0.1 A cm^{-2}, as shown in Fig. 18g, laying the foundation for the exploration of fast ionic conductive adaptive COF SSE for high-energy-density solid-state batteries.

COFs or MOFs with well-ordered channels and stability against phase transition are potential SSEs for rechargeable metal batteries, and their ion conductivity is affected by the Li^+ solvated structure, salt ratio, ion diffusion pathways, *etc.*[46] COFs/MOFs can be functionalized with acidic/anionic groups

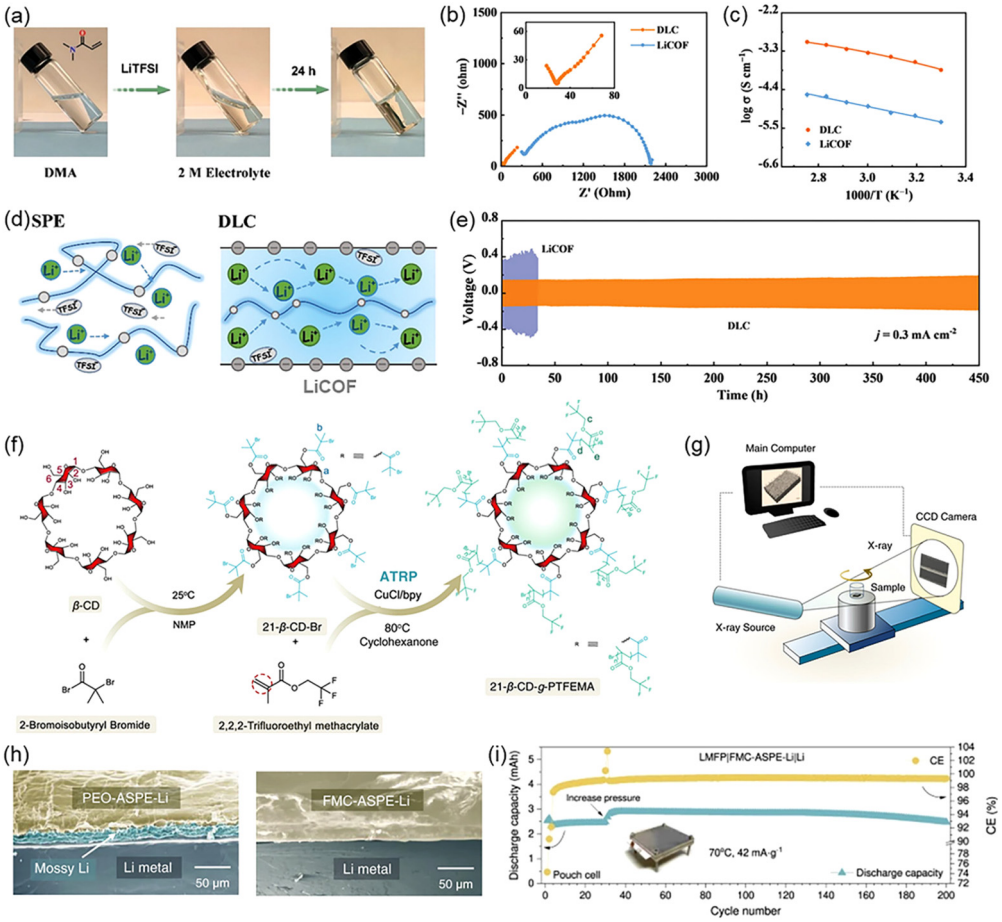

Fig. 17 (a) *In situ* solidification process of the DMA@LiTFSI electrolyte. (b) EIS image of SS|SSE|SS symmetric cells. (c) Ionic conductivities of pristine LiCOF and DLC SSEs. (d) Schematic illustration of the Li^+-transport pathways in conventional SPE and DLC. (e) Comparison of cycling performance of Li|SSE|Li symmetric cell using pristine LiCOF and DLC electrolytes. Reproduced with permission.[186] Copyright 2022, Wiley-VCH GmbH. (f) Synthetic scheme of 21-β-CD-*g*-PTFEMA. (g) Schematic illustration of the working principle of X-ray tomography. (h) SEM images (side view) of the cycled Li|PEO-ASPE-Li|Li and Li|FMC-ASPE-Li|Li symmetric cells. (i) Cycling stability of LMFP|FMC-ASPE-Li|Li pouch cell. Reproduced with permission.[187] Copyright 2022, Nature Publishing Group.

in their nanopores, which may allow them to coordinate/dissociate with single-ions quickly under solvent-free conditions.[95] To improve the ion transfer rate among COF-based SSEs, Li *et al.* demonstrated the porous structure of ionic COF nanosheets (LiCONs) in an all-solid-state organic Li-ion battery (Fig. 19a), which showed an ion conductivity of 10^{-5} S cm^{-1} at −40 °C with enriched ion diffusion pathways, as shown in Fig. 19b.[190] The LiCON-based SSEs with an Li^+ transference number of 0.92 (Fig. 19c) displayed a steady cycling performance over 500 cycles, demonstrating that ionic COFs useful as SSEs and separators in all-solid-state organic batteries. Besides, Sun *et al.* constructed a lithium-sulfonated covalently anchored COF (LiO_3S-COF) as a single-Li-ion conductor (Fig. 19d).[191] Benefiting from the directional ion transfer pathway and single-ion frameworks, LiO_3S-COF2 showed an ion conductivity of 5.47×10^{-5} S cm^{-1}, as shown in Fig. 19e, and the Li|LiO_3S-COF2|Li symmetric cell delivered a steady Li stripping-plating performance for over 450 h (Fig. 19f). Xu's group synthesized 3D anionic COF-based SSEs *via* microwave-assisted method for Li–O_2 batteries (Fig. 19g). The anionic COF-based SSEs with abundant ion transport channels, unique skeleton flexibility and short interfacial transmission impedance showed a high ionic conductivity (2.7×10^{-3} S cm^{-1}).[192] Severe Li^+ polarization and electrolyte depletion were found in the liquid electrolyte; in contrast, the local concentration of Li^+ near the CD-COF-Li SSEs increased significantly, as shown in Fig. 19h, and the current density was uniformly distributed on the Li metal surface. This work provides a new idea for the diversified design of SSEs for LIBs.

In comparison with LIBs, the development of wide-temperature range sodium batteries with SSEs is limited mainly by the slow Na-ion diffusion kinetics.[193] The construction of connected ion diffusion channels in the gel polymer electrolyte (GPE) can offer a promising solution to improve the interface compatibility and ion conductivity of SSEs at expanded temperature. Zhou *et al.* designed an interlock GPE with the introduction of trihydroxymethylpropyl triacrylate (TMPTA) in the liquid electrolyte *via* the *in situ* electrolyte polymerization strat-

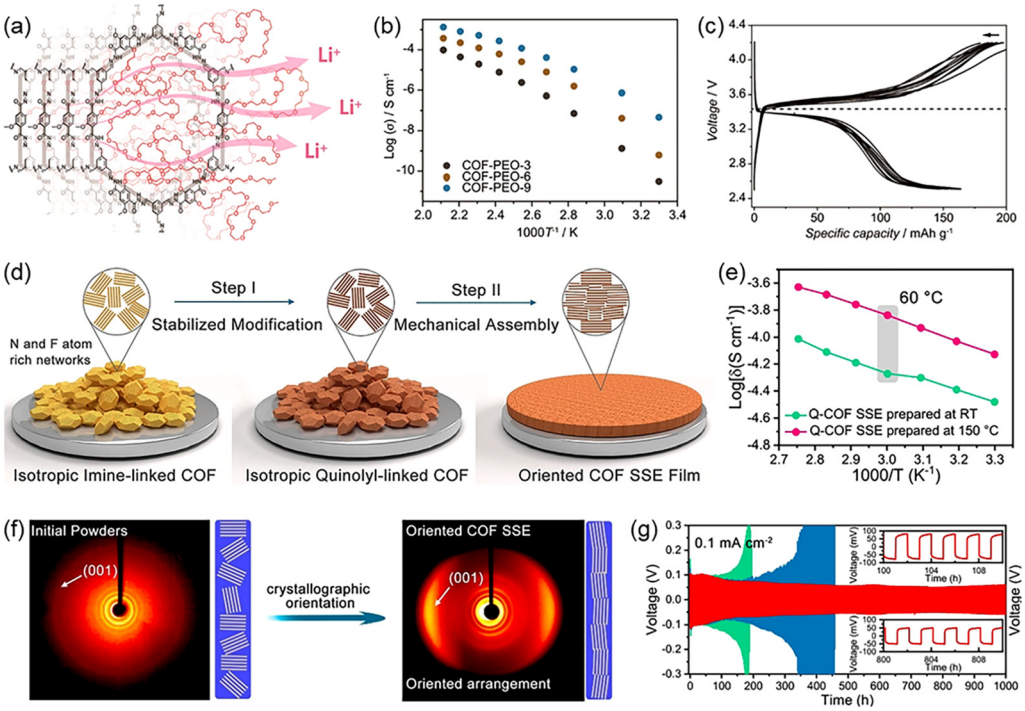

Fig. 18 (a) Illustration of the structure COF-PEO-9. (b) Arrhenius plots of Li^+ conductivity as a function of temperature for COF-PEO-*x*-Li (*x* = 3, 6, 9). (c) Charge/discharge curves of $LiFePO_4$|COF-PEO-9-Li|Li all-solid-state cell at 100 °C. Reproduced with permission.[83] Copyright 2019, the American Chemical Society. (d) Preparation progress of the flexible oriented COF SSE thin films. (e) Ionic conductivities of Q-COF SSE films prepared at different temperatures. (f) Wide-angle X-ray scattering patterns of initial isotropic powders and the oriented Q-COF SSE film. (g) Long-term Li stripping/plating tests of lithium symmetrical cells using imine-linked COF SSE (green line), Q-COF SSE prepared at room temperature (blue line), and Q-COF SSE prepared at 150 °C (red line). Reproduced with permission.[189] Copyright 2021, Wiley-VCH GmbH.

egy, as shown in Fig. 20a.[194] As shown in Fig. 20b and c, the Na|GPE|Na symmetric batteries with interfacial contact showed a good cycling performance over 400 cycles, and the GPE-based cell exhibited a capacity of 98% after 100 cycles when combined with the P2-$Na_{2/3}Ni_{1/3}Mn_{1/3}Ti_{1/3}O_2$ (NMT) cathode. Moreover, Forsyth and colleagues developed a solvent-free SPE with perfluoropolyether-terminated polyethylene oxide (EO10-PFPE)-based block copolymer (Fig. 20d and e) for solid-state sodium metal batteries, and the control homopolymer poly$(PEOA)_{10}$ (EO10-CTRL) was used as the blank electrolyte.[195] The EO10-PFPE-based SPE enabled the assembled symmetric cell to exhibit an ultra-stable cycling performance at 0.5 mA cm^{-2} over 1000 h, which could be attributed to the fast Na^+ transport capacity of the self-assembled nanostructures (Fig. 20f and g). The long-term cycling performance of the all-solid-state Na|EO10-PFPE/PVDF SPE|NVP full cell displayed slight capacity loss after 900 cycles (Fig. 20h), indicating the formation of a stable SEI layer from the PFPE-based SPE.

Ionic COFs with the features of enhanced ionic conductivity, easy chemical modification, and well-defined ion channels are promising ion conductors for SSEs. In the case of the LiO_3S-COF, a lower Li^+ migration barrier (1.0 kcal mol^{-1}) can be obtained along the axial pathway than the planar pathway, and the calculated activation energy of LiO_3S-COF was only 0.13 eV, indicating the superior conductivity of single ionic COFs.[93] Considering the structural designability and framework uniqueness of ionic COFs, as shown in Fig. 21a and b, Sun's research group reported the use of a carboxylic acid sodium-modified polyarylether conjugation COF (NaOOC-COF) as SSEs for a solid-state sodium organic battery.[196] The constructed Na|NaOOC-COF|Na symmetric battery displayed stable Na plating/stripping behavior over 700 h at 0.05 mA cm^{-2} (Fig. 21c), which could be ascribed to the homogeneous Na^+ migration and hopping of Na^+ along the axial pathway in the NaOOC-COF channels. Ionic COF-based SSEs have also been reported in Zn metal batteries. For example, Park *et al.* synthesized a single-ion conducting $SO_3Zn_{0.5}$-COF electrolyte for rechargeable Zn-ion batteries,[197] and $SO_3Zn_{0.5}$-COF improved the stability of the Zn anode surface due to the structural and ion conductive features (Fig. 21d and e). New designs for multiple ionic COFs or MOFs should be further proposed to extend the practical applications of high-performance solid-state alkali/alkaline metal batteries.

Furthermore, quasi-SSEs with a wide electrochemical window, high ionic conductivity, and good mechanical strength are desirable electrolytes for solid-state zinc metal batteries. The well-dispersed multifunctional polymers could be expected to obtain a hydrogen bond network with flexible matrix for efficient Zn ion transport and interface contact.[198]

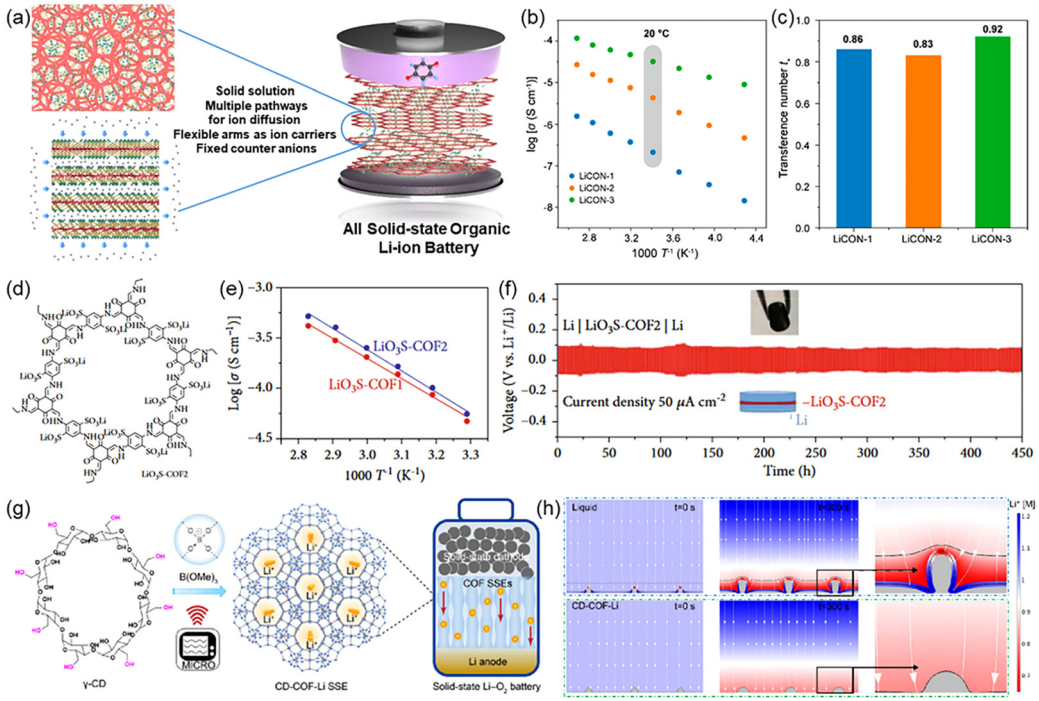

Fig. 19 (a) Schematic illustration of all-solid-state organic Li-ion battery. (b) Arrhenius plots and (c) Li^+ transference number of the as-prepared LiCONs. Reproduced with permission.[190] Copyright 2020, the American Chemical Society. (d) Chemical structure of LiO_3S-COF2. (e) Arrhenius plots of LiO_3S-COF1 and LiO_3S-COF2. (f) Li stripping/plating performance of Li|LiO_3S-COF2|Li symmetric cell at 50 μA cm^{-2}. Reproduced with permission.[191] Copyright 2022, Yongjiang Sun *et al.* (g) Process for the preparation of CD-COF-Li-SSE in a solid-state Li-O_2 battery. (h) Finite element modelling simulations of Li^+ concentration distribution and Li deposition in liquid electrolyte and CD-COF-Li-SSE. Reproduced with permission.[192] Copyright 2022, Wiley-VCH GmbH.

For example, polyzwitterionic hydrogel electrolytes are promising platforms to design safe, economic, and stable quasi-solid-state zinc metal batteries. The charged groups of the zwitterionic polymer not only homogenized the Zn^{2+} distribution, but also improved the ionic conductivity of an SPE to 32.0 mS cm^{-1} at room temperature.[199] Inspired by the multiple functional groups and porous features of MXenes, Zhi's group developed a method for the chemical grafting of MXenes to induce abundant F–H hydrogen bond interactions between the highly grafted PMA and poly(vinylidene fluoride co-hexafluoropropylene) (PH) matrix in SPEs, improving the ionic conductivity (2.69×10^{-4} S cm^{-1}) of the PH/PMA/MXene SPE in the dendrite-free Zn plating/stripping process.[200] Moreover, Feng *et al.* constructed a SPE by combining an MXene and PH/Zn $(OTf)_2$ network (PH/MXene-SPE), as shown in Fig. 22a.[201] The designed PH/MXene-SPE improved the cycling performance of the Zn|PH/MXene-SPE|Zn symmetric cell for over 2500 h (Fig. 22b), which was attributed to the enhanced ionic conductivity and regulated the interphase chemistry and Zn deposition. To explore the realistic application of zinc air batteries, Lee's research group presented a 1-Ah-class all-solid-state zinc-air pouch cell with a (101)-facet copper phosphosulfide [CPS (101)] cathode, anti-freezing chitosan- biocellulosic (CBC) electrolyte and zinc metal anode (Fig. 22c and d).[202] The hydroxide CBC electrolyte exhibited ultrahigh ionic conductivity (86.7 mS cm^{-1} at 25 °C) and stable Zn stripping/plating behavior in a cell-level all-solid-state zinc-air battery (Fig. 22e–g), which potentially paved the way for fast-charging and safe high-power/energy-density batteries in electric and wearable devices.

Moreover, magnesium/aluminum metal batteries also face the issues of self-corrosion, insulating passivation films, and irreversible stripping/plating behavior, which limit their application in specific electrolytes.[203] With the rapid development of solid-state electrolytes, polymer electrolytes are emerging in the studies of magnesium/aluminum metal batteries, offering a novel solution to improve the reversible stripping/plating and interfacial compatibility for magnesium/aluminum metals. For example, Cui and colleagues presented a robust self-standing polyepichlorohydrin-based polymer electrolyte for high-safety magnesium metal batteries.[204] The rationally designed single-ion cross-linked network and triglyme-plasticized structure endowed the polymer electrolyte with a remarkable Mg^{2+} transfer number (0.79) and reversible Mg plating/stripping behavior (stably cycling for 150 h at 0.05 mA cm^{-2}). Besides, the Mo_6S_8||Mg full batteries with this single-ion polymer electrolyte exhibited superior thermal stability and high safety under extreme conditions (150 °C). Additionally, to prevent the self-corrosion and improve the utilization efficiency of Al metal in alkaline electrolyte, Tang's research group reported a dual-electrolyte consisting of polyacrylic acid hydrogel and aqueous electrolyte (4 M KOH) for an Al-air

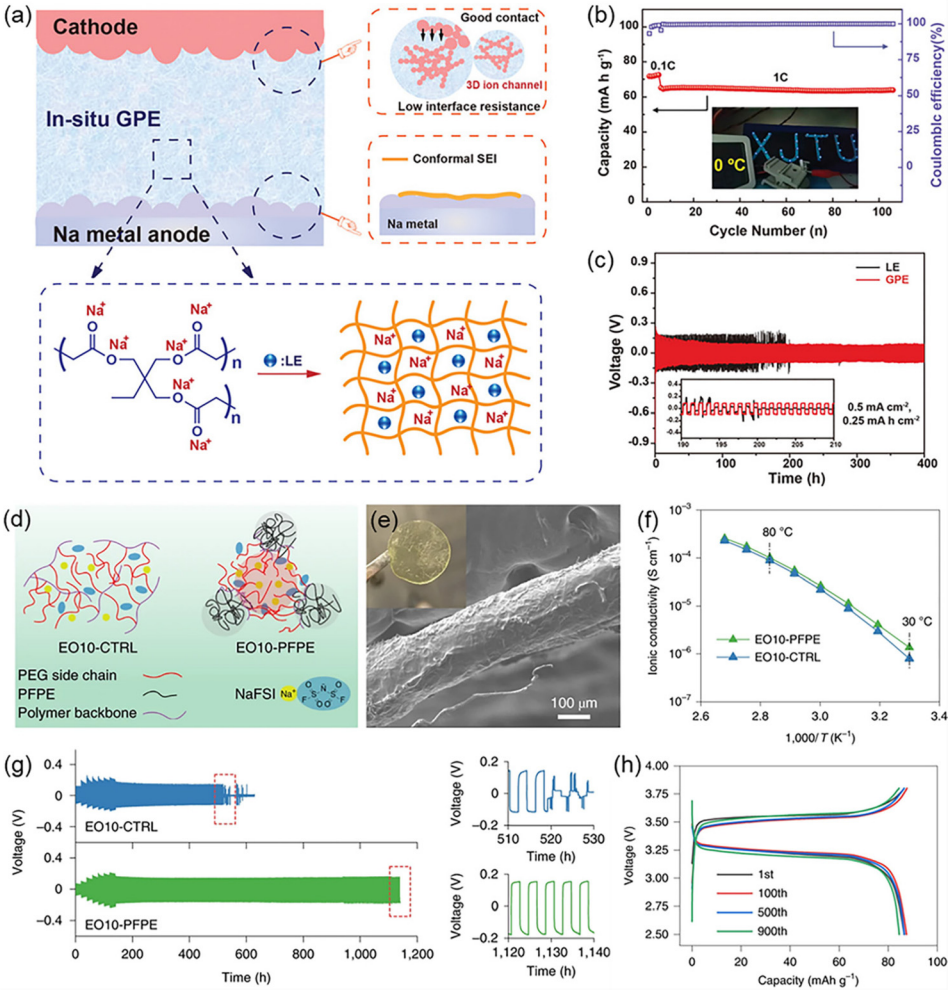

Fig. 20 (a) Schematic illustration of *in situ* GPE structure. (b) Cycle stability of Na|GPE|NMT cell at 1 C. (c) Na stripping/plating performances of symmetric batteries with GPE and liquid electrolytes. Reproduced with permission.[194] Copyright 2022, Wiley-VCH GmbH. (d) Schematic profile of the self-assembled nanostructures in SPEs. (e) Cross-sectional SEM image of EO10-PFPE composite solid polymer electrolyte. (f) Ionic conductivity of PFPF-based and CTPL-based electrolytes at 30 °C. (g) Long-term sodium plating/stripping tests in PFPF-based and CTPL-based electrolytes at 0.5 mA cm^{-2}. (h) Charge/discharge curves of all-solid-state Na|EO10-PFPE/PVDF SPE|NVP cell at 2 C. Reproduced with permission.[195] Copyright 2022, Nature Publishing Group.

battery.[205] Consequently, the dual-electrolyte- constructed Al-air battery displayed an enhanced discharge capacity (1769.0 mA h g^{-1}) and suppressed polarization at 20 mA cm^{-2} in comparison to the single electrolytes. Therefore, the dual-electrolyte system could suppress the self-corrosion of the Al anode and without losing its high ionic conductivity and decreased polarization merits.

4.4. Other applications

4.4.1. Hosts for lithium/sodium sulfur batteries. Lithium–sulfur batteries (LSBs) offer the characteristics of high energy density, low cost, low toxicity, and environmental friendliness, making them promising energy storage devices.[206,207] The shuttling effect of lithium polysulfides and slow redox kinetics cause irreversible capacity loss and limited sulfur utilization, making it a challenge to apply LSBs on a broad scale. Hence, an effective method is developing stable sulfur-containing cathode materials.[208] For loading sulfur and immobilizing lithium polysulfides during electrochemical processes, MOFs and COFs with large specific surface areas and clearly defined pores are regarded as the promising hosts.[185] Zhang *et al.* reported the preparation of a 3D porous S-ZIF-8 and CNT hybrid structure.[209] Large CNT sponges were directly used as templates and S-ZIF-8 particles were uniformly grafted on S-ZIF-8@CNTs (Fig. 23a and b). MOF particles with a 3D porous structure could be used to achieve a high area sulfur loading. By combining physical confinement and chemical bonding, MOFs could serve as a functional sulfur host to hold polysulfide intermediates *in situ*, which offered effective charge transport pathways linked with CNT networks. In 2021, Liu *et al.* evenly coated CNTs with a conjugate micro/meso-porous polymer, which not only enabled the adsorption of lithium polysulfides, but also accelerated the catalytic transformation of LBSs.[210] FOMs with high stable capacity and out-

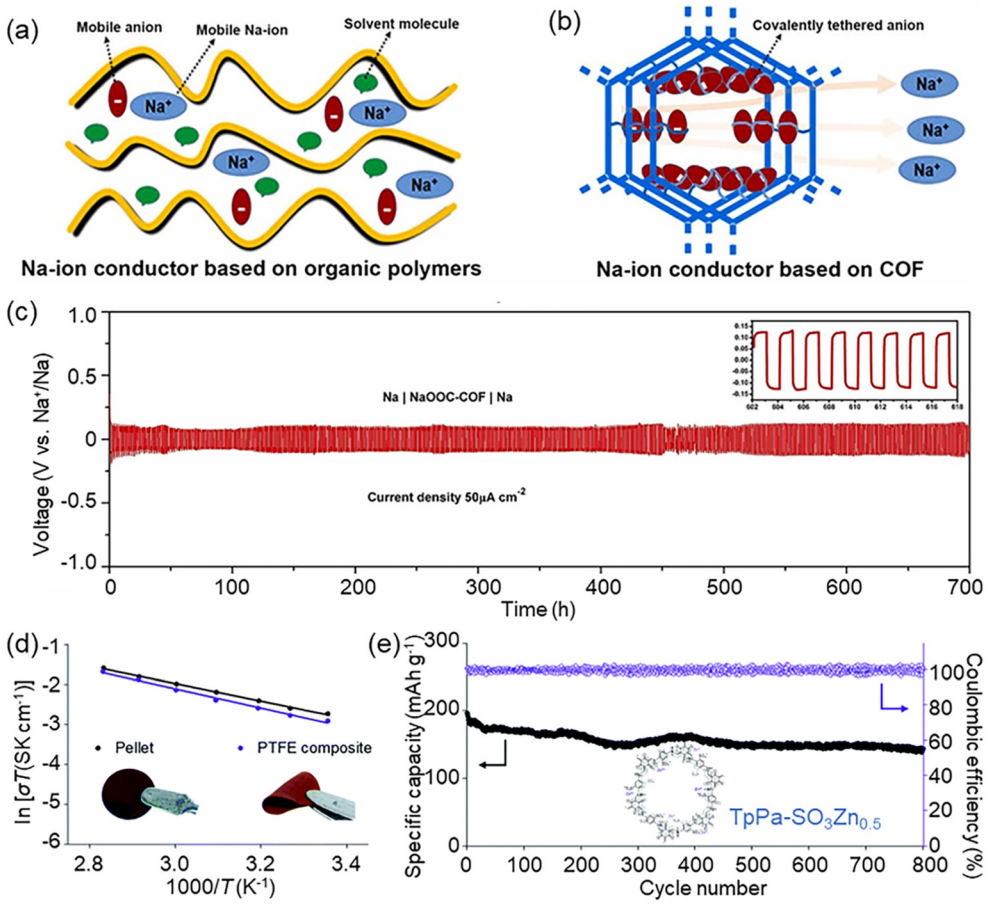

Fig. 21 Comparison of Na^+ conductor based on (a) organic polymers and (b) ionic COF. (c) Na stripping/plating behavior of Na|NaOOC-COF|Na symmetrical cell for 1 h per cycle. Reproduced with permission.[196] Copyright 2021, Elsevier B.V. (d) Arrhenius plots of $SO_3Zn_{0.5}$-COF-based pellet with/without PTFE. The inset images are the $SO_3Zn_{0.5}$-COF pellet and the $SO_3Zn_{0.5}$-COF-PTFE composite, respectively. (e) Cycling stability of Zn|$SO_3Zn_{0.5}$-COF|MnO_2 cell. The inset is the chemical structure of $SO_3Zn_{0.5}$-COF. Reproduced with permission.[197] Copyright 2020, Sodam Park *et al.*

standing cycle stability are promising composite cathodes for advanced energy storage systems.

Similar to MOFs, the porous structure of COFs also provides space for energy storage. However, the physical blocking of sulfur in their channels is not enough to inhibit the shuttle effect of the lithium polysulfide intermediates, resulting in the poor cycling performance of LSBs. Feng's research group designed a flexible and self-standing MXene/COF framework for Li metal anodes, with the lithiophilic COF distributing among the MXene framework to induce the uniform Li nucleation/deposition.[211] The MXene/COF-based Li||S cells showed enhanced electrochemical stability (with a capacity retention of 73.8% after 300 cycles) and Coulombic efficiency, owing to the regulation of the COF seeds for Li^+ flux homogenization and low nucleation barrier. Moreover, Xu and colleagues reported a new imine-linked TFPPy-ETTA-COF host *via* the solvothermal reaction between 1,3,6,8-tetrakis(4-formylphenyl) pyrene (TFPPy) and 4,4′,4″,4‴-(ethene-1,1,2,2-tetrayl)tetraaniline (ETTA), which was used to suppress the shuttle effect of lithium polysulfides.[212] The imine bonds in S@TFPPy-ETTA-COF could cause sulfur to polymerize in the COFs, forming polysulfide chains that could cling to the channel walls, which showed the good cycling performance of lithium–sulfur batteries (Fig. 23c and d).

Sodium-sulfur batteries have a similar reaction mechanism to LSBs, but they face greater challenges, owing to their low reversible capacity and fast capacity decay. Ye *et al.* demonstrated that the dynamic electrons of metals in MOFs can regulate the interaction between polysulfides and MOFs during cycling, which is conducive to the rapid conversion of polysulfides. Polysulfide intermediates can be confined in the porous structure of MOFs, reducing their shuttle effect.[213] Besides, Huang *et al.* employed $Fe(CN)_6^{4-}$-doped polypyrrole as a cationic reservoir, which exhibited strong adsorption to the sodium polysulfides and short chains, effectively reducing the loss of sodium polysulfides (Fig. 23e).[214] During reverse charging, the Fe redox centers could reduce the Na_2S activation energy barrier and promote the reversibility of Na_2S deposition. Consequently, the constructed Na–S cell exhibited a high reversible capacity of 1071 mA h g^{-1} and a capacity retention of 72.8% after 200 cycles, indicating the confined electrocatalytic effect of $Fe(CN)_6^{4-}$-doped polypyrrole for high-efficiency sulfur electrochemistry.

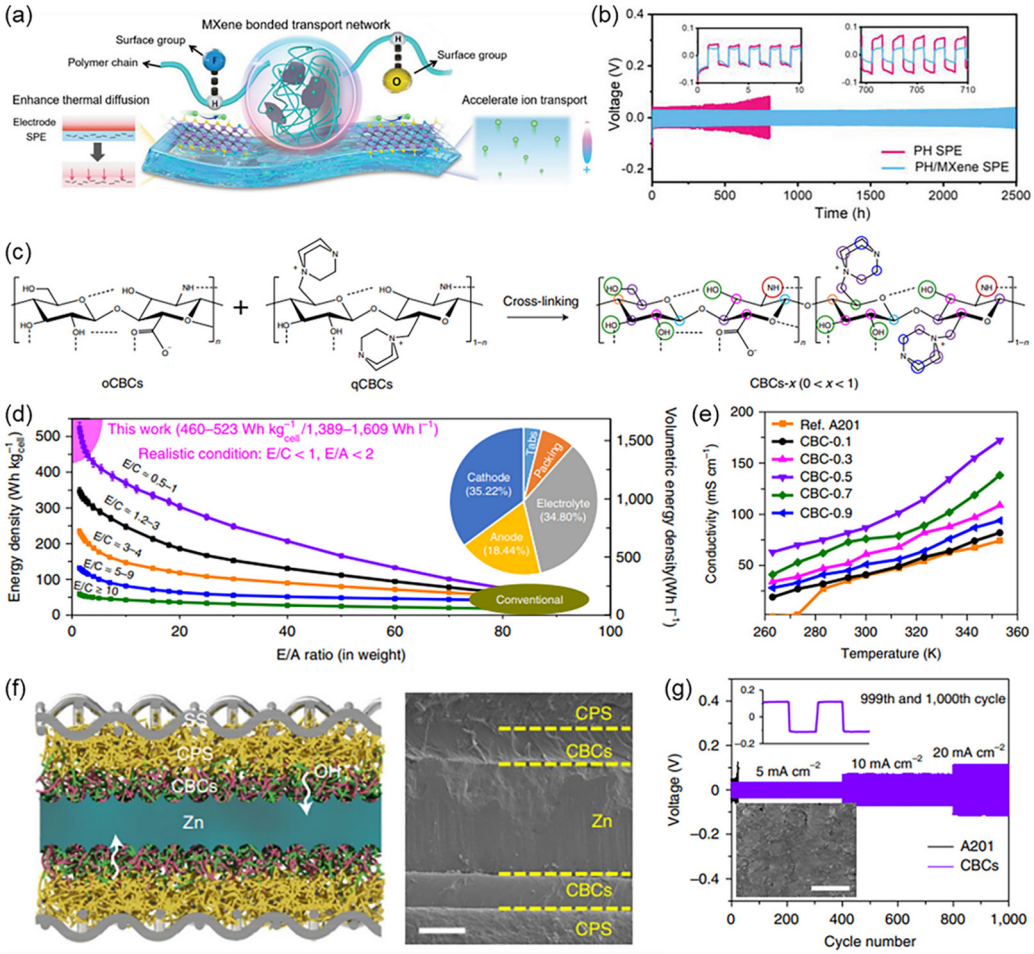

Fig. 22 (a) Schematic illustration of PH/MXene-SPE. (b) Cycling performance of Zn stripping/plating processes in Zn|PH-SPE|Zn and Zn|PH/MXene-SPE|Zn symmetric cells. Reproduced with permission.[201] Copyright 2022, Wiley-VCH GmbH. (c) Fabrication process of CBC electrolytes. (d) Relationship between the E/A E/C ratios and the realistic cell-level energy densities of this work and other conventional zinc batteries. The inset is the optimal weight distributions of the ampere-hour-scale zinc-air pouch cell. (e) Hydroxide ion conductivity of SPEs with different portions of CBC. (f) Illustration of the configuration the an all-solid-state zinc-air pouch cell and its corresponding cross-sectional SEM image. (g) Rate performance of the symmetric Zn|CBC|Zn cell. Reproduced with permission.[202] Copyright 2021, Nature Publishing Group.

4.4.2. FOM-based separators. As early as 2016, Bai *et al.* firstly proposed the use of MOFs as separators in LSBs.[215] MOF-modified separators can function as an ionic sieve, selectively screening Li^+ and inhibiting the shuttle effect of polysulfides. Based on this study, an MOF gel separator was designed to match the organic electrode material-5,5′-dimethyl-2,2′-bis-*p*-benzoquinone (Me_2BBQ) (Fig. 24a–c).[216] The micropore size of zeolitic imidazole framework-8 (ZIF-8) was sufficient to block the passage of the Li–Me_2BBQ complex, which confirmed the regulation effect of the selective MOF gel separator to the Me_2BBQ^{n-} intermediates. The majority of research on separators concentrated on minimizing the "shuttle effect" in LSBs, while only a few studies focused on stabilizing the metal anode in lithium metal batteries (LMBs). Hao *et al.* developed a well-designed MOF separator with Nafion, which could realize ion regulation and solve the lithium dendrite problem.[217] The $-NH_2$ groups and the intrinsic nanochannels in the MOF facilitated Li^+ migration, and the Nafion component with negatively charged SO_3^- groups could inhibit the migration of PF_6^- by electrostatic interactions in the separator, thus achieving uniform lithium deposition (Fig. 24d). Therefore, MOFs offer good solvation performances, while their huge mass and density limit the energy density of the overall LMBs.

Notably, COFs with tunable structure, thermal stability, and low density have become alternative candidates.[218] Yang *et al.* designed an excellent self-supporting TPB-BD$(OH)_2$-COF/PVDF separator, which could induce the uniform distribution of Li^+ and greatly inhibit dendrite growth.[219] COFs with hydroxyl functional groups will interact with the electrolyte components to form a hydrogen bond network, showing a good desolvation effect and limited side reactions in the resultant separator. COF materials have also been applied in Na–S cells to improve their cycle performance. For example, Yin *et al.* synthesized a COF film with 1,3,5-triformylbenzene and azobenzene-modified hydrazide linkers (Azo-TbTh), which could inhibit the

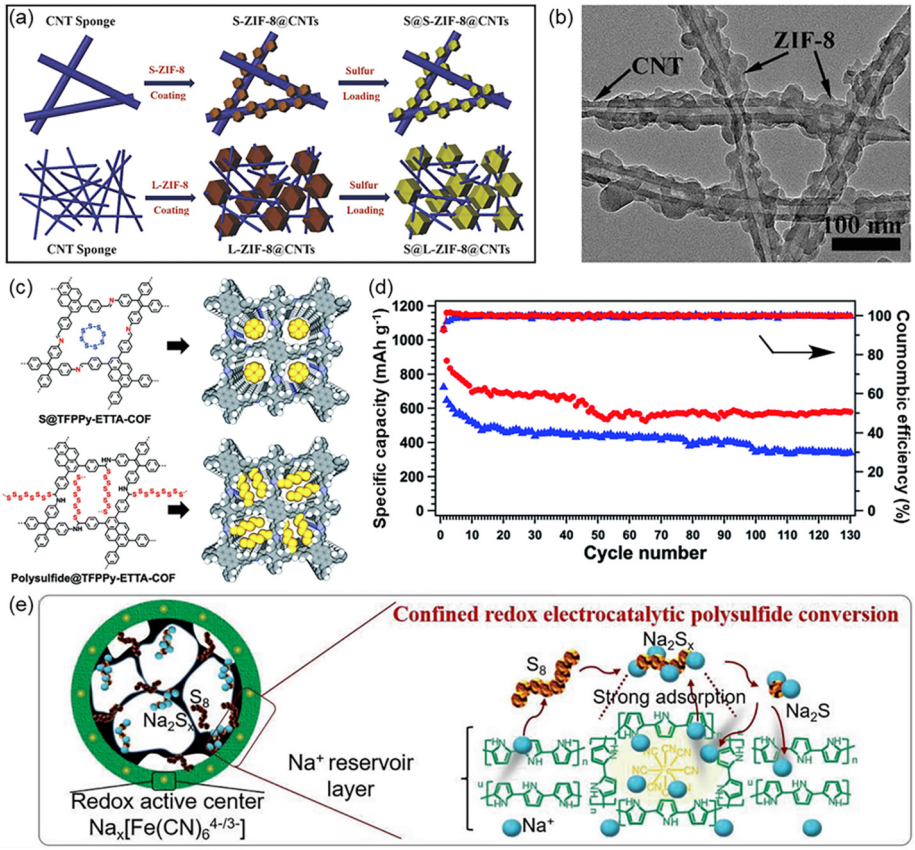

Fig. 23 (a) Schematic of S-ZIF-8 growth and sulfur loading process on CNT skeleton. (b) TEM image of S-ZIF-8@CNTs. Reproduced with permission.[209] Copyright 2018, Wiley-VCH GmbH. (c) Schematic illustration of S_8 and polysulfide chains limited into TFPPy-ETTA-COF *via* physical isolation and chemical bonding, respectively. (d) Cycling stability of polysulfide@TFPPy-ETTA-COF (red dot) and S@TFPPy-ETTA-COF (blue dot) cathodes at 0.1 C. Reproduced with permission.[212] Copyright 2019, Fei Xu *et al.* (e) Schematic illustration of the redox active center to catalyze the conversion rate of sodium polysulfides. Reproduced with permission.[214] Copyright 2021, Wiley-VCH GmbH.

"shuttling effect" of sodium polysulfides.[220] The functional azo groups of the Azo-TbTh COF film served as a redox center to interact with Na^+ in a reversible manner, which acted as an Na^+ jump site to promote Na^+ migration (Fig. 24e). Utilizing this thin Azo-TbTh COF layer as a separator, the specific capacity and rate performance of the Na–S cell were greatly improved with a capacity decay rate of 0.036% for each cycle during 1000 cycles (Fig. 24f).

4.4.3. FOM-based redox flow batteries. Aqueous redox flow batteries (ARFBs) are promising alternatives for large-scale electricity energy storage devices to realize the effective utilization of the intermittent renewable energy, but they suffer from a short cycle life and limited capacity.[221] Organic redox–active molecules with good structural tunability, electrochemical reversibility, and reaction rates offer the merits of enhanced capacity, eco-friendly, and fast redox reaction kinetics for ARFBs.[222] Generally, organic molecules (such as quinone, viologen, azo, phenazine, phenothiazine, TEMPOs, and their derivatives) with high solubility in electrolyte and highly reversible redox-active sites are ideal electroactive materials and charge/electron transfer carriers in ARFBs.[223] Novel organic salts are designed by molecular engineering, for example, Yu's research group reported the use of azobenzene-based molecules with hydrophilic groups as an anolyte for ARFBs, as shown in Fig. 25a.[224] The highly soluble azobenzene-based molecules with amino and sulfonic groups displayed outstanding solvation behavior and fast redox chemistry, and the ARFBs with 0.8 M active material exhibited a high anolyte capacity of 41.5 Ah L^{-1} and high energy efficiency (Fig. 25b).

Moreover, Wang and colleagues designed a biomimetic high-capacity phenazine-based anolyte for ARFBs, and the soluble phenazine molecular shifted its redox potential by about 400 mV.[225] The ARFBs demonstrated a reversible anolyte capacity of 67 Ah L^{-1} and a capacity retention of 99.98% per cycle over 500 cycles. Therefore, these results are critical towards the further development of ARFB technologies with practical applications. Recently, Wang's group reported dihydroxyanthraquinone (DHAQ)-based alkaline electrolytes for ARFBs *via* molecular engineering, and 1,5-DHAQ molecule undergoes a hydrogen bond-mediated degradation mechanism during the charge/discharge process (Fig. 25c and d).[226] Afterwards, the assembly redox flow batteries exhibited an output capacity of nearly 570 mA h after cycling for 1100 h (Fig. 25e), owing to the combination of redox-active polymer-

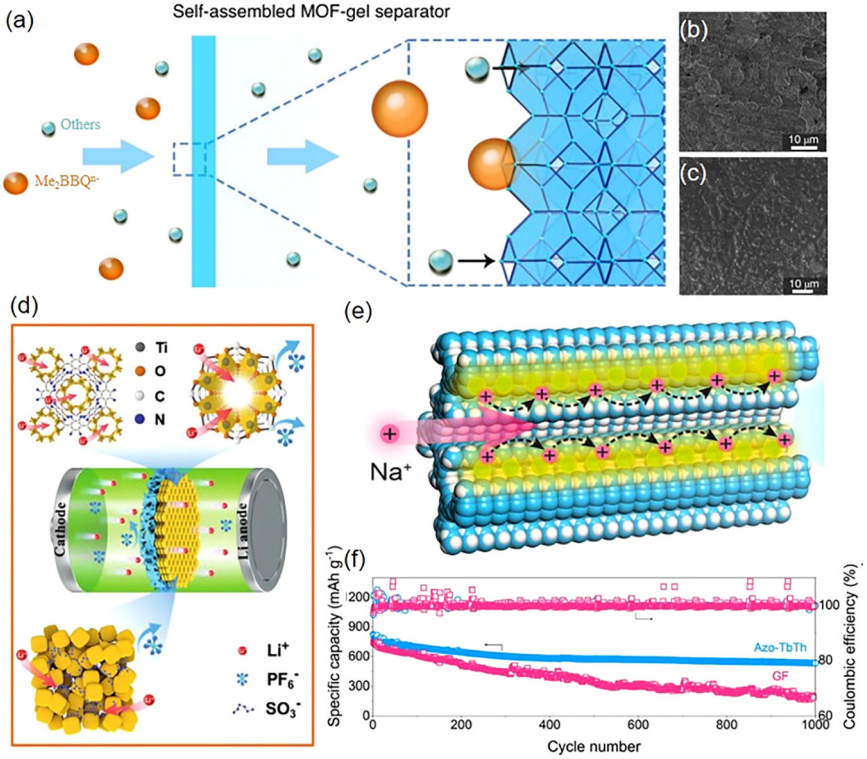

Fig. 24 (a) Schematic illustration of MOF-gel separator for limiting Me_2BBQ^{n-}. Comparison of SEM images of the deposition morphology of lithium metal electrodes using a common separator (b) and MOF-gel separator (c). Reproduced with permission.[216] Copyright 2020, Springer Nature. (d) Schematic diagram of MOFs@PP separator regulating Li^+ and anion migration in LMBs. Reproduced with permission.[217] Copyright 2021, Wiley-VCH GmbH. (e) Schematic profile of Na^+ rapid migration mechanism in Azo-TbTh separator. (f) Cyclic stability of Na–S batteries assembled with Azo-TbTh and GF as separators at 1 C. Reproduced with permission.[220] Copyright 2022, the American Chemical Society.

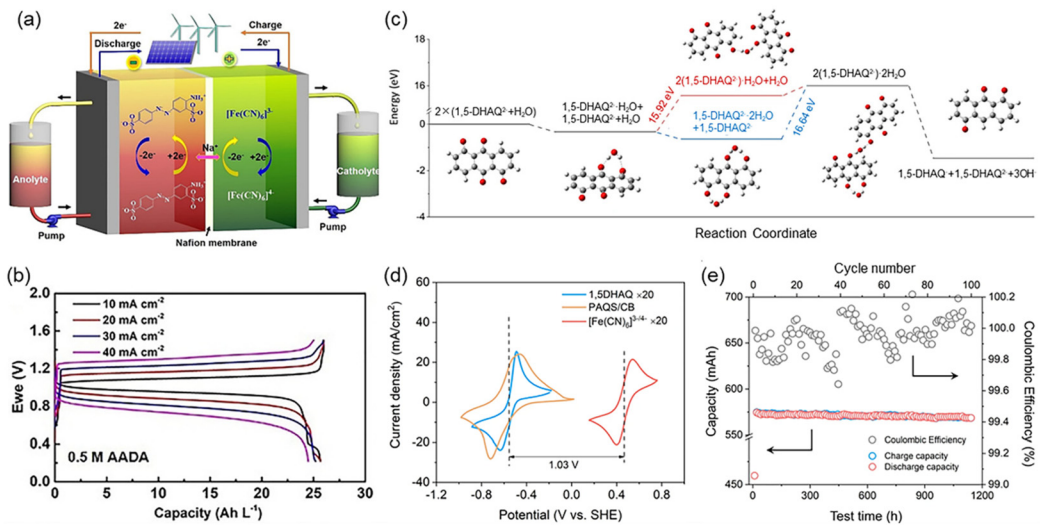

Fig. 25 (a) Schematic illustration of the working process of ARFBs. (b) Rate performance of ARFBs with 0.5 M functional azobenzene-based anolyte. Reproduced with permission.[224] Copyright 2022, Wiley-VCH GmbH. (c) Calculated energy changes of 1,5-DHAQ at different coordinated states. (d) Cyclic voltammetry curves of 1,5-DHAQ, PAQS/CB, and $[Fe(CN)_6]^{3-/4-}$. (e) Long-term cycling performance of the assembled flow cell. Reproduced with permission.[226] Copyright 2022, Nature Publishing Group.

based capacity-boosting composite anolyte and $[Fe(CN)_6]^{3-/4-}$ alkaline catholyte. The DHAQ-based anolyte delivered highly electrochemical reversibility (over 1000 cycles) and rapid reaction rates in conjunction with PAQS/CB granules, which provided a promising avenue for the further exploration of solid-state organic-based ARFBs.

5. Conclusion and outlooks

In summary, we summarized the recent advances in FOM-based interfacial engineering for metal anode protection of rechargeable batteries in liquid/solid-state electrolytes. Organic additives favor the formation of uniform SEI layer and maintaining the structural stability of metal anodes during metal plating/stripping process.[227] Additionally, FOMs with stable framework, regular pores, modifiable structures, and abundant active sites can mitigate the inherent problems such as dendrite growth, side reactions, and even volume change confronted by metal anodes.[17,26] Moreover, the application of polymers and 2D porous materials in gel/SSEs and other areas was also presented, and thus it is expected that more effort will be devoted to the development of FOMs in rechargeable batteries.[218] However, most of the previous studies on FOMs have focused on improving the metal interface, especially in Li metal batteries.[14,21,101,133] They also appeared in the anodic protection of Na, K, Zn, and Mg metal batteries, but the studies are still in their infancy.[160] More effort should be devoted to the structural design and interfacial engineering of FOMs for SEI modification and SSEs to promote the practical application of high-energy-density rechargeable metal batteries. As an outlook, the further exploration of FOMs for rechargeable batteries are emphasized below.

5.1. Structure design of novel FOMs

FOMs with different structures and functional groups will make a difference in the deposition behaviors of metal anodes, and thus muti-functional COFs/MOFs and their derivatives should be explored to regulate the metal plating/stripping process and ion transfer behavior, improving the overall electrochemical performance of rechargeable metal batteries. Moreover, polymers with flexible structures and metallophilic groups are potential substrates to realize the uniform distribution of ion flux and accommodation of the volume expansion, which are also suitable for COFs/MOFs and their derivatives with porous structure and rigid channels. However, most of the synthesis routes for COFs and MOFs are complex, time-consuming, and even require harsh conditions, and thus FOMs with simple and efficient preparation processes are worthy of further exploration. COFs/MOFs with poor flexibility and processability can be improved by bottom-up structural design, combination with flexible polymers, and *in situ* formation on the metal surface. In addition, the inherent physical properties of FOMs such as mechanical strength, structural frame and porosity are also important factors affecting the cycling performance of rechargeable metal batteries. Therefore, in conjunction with machine-learning methods and sophisticated synthetic techniques, finding and synthesizing more economical and efficient materials without sacrificing the function of materials will effectively promote the application scope of materials in secondary batteries.

5.2. Application of FOMs in anode protection

With the development of secondary metal (Li, Na, K, Zn, Mg, Al, *etc*.) batteries in recent years, the exploration and utilization of FOMs for metal anode protection have become more extensive and comprehensive.[227] However, the current studies mainly focus on making use of the flexible structure and functional groups for anode protection, while few studies refer to the ion transfer ways and inner mechanisms. FOMs with redox-active groups are emerging for SEI modification for metal anode protection, having potential effects on accelerating the ion transfer and metal deposition/stripping behavior. Besides, the broader application of FOMs in different battery systems also needs to be explored with different reaction mechanisms. Therefore, the preparation of FOM-based protective layers with tight structure, low grain boundary resistance, and rapid ion transport characters has become an urgent pursuit of researchers.

5.3. Modification of gel/solid state electrolytes

The high crystallinity of polymers affects their ionic conductivity as SEI films or SSEs, and thus reducing the crystallinity and regulating the ion transfer rates of polymer solid electrolytes are an urgent concern. In contrast, the applications of COFs/MOFs and their derivatives with periodic structure and tunable functionality are foreseeable in SSEs, while the related research in SSEs has been gradually emerging in secondary metal batteries recently. The development of COFs/MOFs in SSEs is closely associated with their structural designability and synthesis technology, favoring the construction of SSEs with modified ion transport channels and interface compatibility. Researchers need to explore ways to combine FOMs with electrolytes more evenly and design SSEs with a wide voltage window to match the high-voltage cathodes, achieving a more reasonable ion transport path to realize the efficient utilization of FOMs.

5.4. Application of FOMs in other areas

FOMs have been employed for the construction of quasi-SSEs, the modification of separators, sulfur hosts, and redox electrolytes, *etc*., but the research in emerging secondary batteries is still in its infancy. The porous structures of FOM-separators/hosts can limit the shuttling effect of polysulfides and achieve rapid transformation of intermediates, realizing their rapid conversion and enhanced cycle life in Li/Na sulfur batteries. Moreover, FOM-based separators with flexible structures are promising candidates for redox flow batteries, limiting the shuttling effect of some soluble redox intermediates. However, the physical/chemical adsorption between materials and polysulfides may not be stable, and the FOMs may be consumed, fall off or dissolve in the electrolytes during the battery operation, which are intractable issues that remain to be further explored. Therefore, the outstanding performance and related ion transport mechanism of FOMs should be determined in rechargeable secondary batteries.

Therefore, FOMs with multifunctional properties are promising candidates for stabilizing the metal interface, distributing the uniform ion flux, and accelerating the rapid transport of target ions. How to utilize the potential properties of FOMs

to satisfy the practical requirements of rechargeable metal batteries is a crucial point in the near future.

Conflicts of interest

The authors declare no competing financial interests.

Acknowledgements

This work was supported by the National Natural Science Foundation of China (21773055 and U22A20437), Joint Fund of Science and Technology R&D Plan of Henan Province (222301420005), Key Scientific Research Project of Higher Education in Henan Province (22A150004), and China Postdoctoral Science Foundation under Grant (2021M701069).

References

1 Y. Guo, H. Li and T. Zhai, *Adv. Mater.*, 2017, **29**, 1700007.
2 M. Baumann, L. Barelli and S. Passerini, *Adv. Energy Mater.*, 2020, **10**, 2001002.
3 X. Zhang, R. Lv, W. Tang, G. Li, A. Wang, A. Dong, X. Liu and J. Luo, *Adv. Funct. Mater.*, 2020, **30**, 2004187.
4 D. Lin, Y. Liu and Y. Cui, *Nat. Nanotechnol.*, 2017, **12**, 194–206.
5 M. Winter, B. Barnett and K. Xu, *Chem. Rev.*, 2018, **118**, 11433–11456.
6 N. Yabuuchi, K. Kubota, M. Dahbi and S. Komaba, *Chem. Rev.*, 2014, **114**, 11636–11682.
7 F. Wang, O. Borodin, T. Gao, X. Fan, W. Sun, F. Han, A. Faraone, J. A. Dura, K. Xu and C. Wang, *Nat. Mater.*, 2018, **17**, 543–549.
8 F. Wan, X. Zhou, Y. Lu, Z. Niu and J. Chen, *ACS Energy Lett.*, 2020, **5**, 3569–3590.
9 Q. Li, A. Chen, D. Wang, Y. Zhao, X. Wang, X. Jin, B. Xiong and C. Zhi, *Nat. Commun.*, 2022, **13**, 3699.
10 K. Xu, *J. Power Sources*, 2023, **559**, 232652.
11 J. Popovic, *Nat. Commun.*, 2021, **12**, 6240.
12 C. Yang, K. Fu, Y. Zhang, E. Hitz and L. Hu, *Adv. Mater.*, 2017, **29**, 1701169.
13 C. Chu, R. Li, F. Cai, Z. Bai, Y. Wang, X. Xu, N. Wang, J. Yang and S. Dou, *Energy Environ. Sci.*, 2021, **14**, 4318–4340.
14 C. Bao, B. Wang, P. Liu, H. Wu, Y. Zhou, D. Wang, H. Liu and S. Dou, *Adv. Funct. Mater.*, 2020, **30**, 2004891.
15 Q. Li, J. Zhang, Y. Zeng, Z. Tang, D. Sun, Z. Peng, Y. Tang and H. Wang, *Chem. Commun.*, 2022, **58**, 2597–2611.
16 P. Zhao, G. Kuang, R. Qiao, K. Liu, F. B. Ajdari, K. Sun, C. Bao, M. Salavati-Niasari and J. Song, *ACS Appl. Energy Mater.*, 2022, **5**, 10141–10148.
17 T. Wang, Y. Hua, Z. Xu and J. S. Yu, *Small*, 2022, **18**, 2102250.
18 J. Zhao, Y. Ying, G. Wang, K. Hu, Y. D. Yuan, H. Ye, Z. Liu, J. Y. Lee and D. Zhao, *Energy Storage Mater.*, 2022, **48**, 82–89.
19 Y. Wang, H. Sun, N. Li, K. Chen, X. Yang, H. Liu, G. Zheng, J. Liu, Z. Wu, L. Zhai and L. Mi, *ACS Appl. Energy Mater.*, 2022, **5**, 2375–2383.
20 P. Jaumaux, J. Wu, D. Shanmukaraj, Y. Wang, D. Zhou, B. Sun, F. Kang, B. Li, M. Armand and G. Wang, *Adv. Funct. Mater.*, 2021, **31**, 2008644.
21 J. Kang, N. Deng, Y. Liu, Z. Yan, L. Gao, H. Xiang, L. Zhang, G. Wang, B. Cheng and W. Kang, *Energy Storage Mater.*, 2022, **52**, 130–160.
22 L. Fan, S. Wei, S. Li, Q. Li and Y. Lu, *Adv. Energy Mater.*, 2018, **8**, 1702657.
23 B. Horstmann, J. Shi, R. Amine, M. Werres, X. He, H. Jia, F. Hausen, I. Cekic-Laskovic, S. Wiemers-Meyer, J. Lopez, D. Galvez-Aranda, F. Baakes, D. Bresser, C.-C. Su, Y. Xu, W. Xu, P. Jakes, R.-A. Eichel, E. Figgemeier, U. Krewer, J. M. Seminario, P. B. Balbuena, C. Wang, S. Passerini, Y. Shao-Horn, M. Winter, K. Amine, R. Kostecki and A. Latz, *Energy Environ. Sci.*, 2021, **14**, 5289–5314.
24 Q. Wang, B. Liu, Y. Shen, J. Wu, Z. Zhao, C. Zhong and W. Hu, *Adv. Sci.*, 2021, **8**, 2101111.
25 P. Liu, H. Yi, S. Zheng, Z. Li, K. Zhu, Z. Sun, T. Jin and L. Jiao, *Adv. Energy Mater.*, 2021, **11**, 2101976.
26 J. Huang, X. Liu, W. Zhang, Z. Liu, H. Zhong, B. Shao, Q. Liang, Y. Liu, W. Zhang and Q. He, *Chem. Eng. J.*, 2021, **404**, 127136.
27 S. Gao, Z. Li, N. Liu, G. Liu, H. Yang and P. Cao, *Adv. Funct. Mater.*, 2022, **32**, 2202013.
28 S. Gao, F. Sun, N. Liu, H. Yang and P.-F. Cao, *Mater. Today*, 2020, **40**, 140–159.
29 S. Huo, Y. Zhang, Y. He, W. Fan, Z. Hu, W. Bao, X. Jing and H. Cheng, *J. Phys. Chem. Lett.*, 2023, **14**, 16–23.
30 C. Zhang, A. Wang, J. Zhang, X. Guan, W. Tang and J. Luo, *Adv. Energy Mater.*, 2018, **8**, 1802833.
31 X. Cui, H. Dong, S. Chen, M. Wu and Y. Wang, *Batteries Supercaps*, 2021, **4**, 72–97.
32 X. Li, M. Lv, Y. Tian, L. Gao, T. Liu, Q. Zhou, Y. Xu, L. Shen, W. Shi, X. Li, Y. Lu, X. Liu and S. Xiao, *Nano Energy*, 2021, **87**, 106214.
33 C. Wei, L. Tan, Y. Zhang, K. Zhang, B. Xi, S. Xiong, J. Feng and Y. Qian, *ACS Nano*, 2021, **15**, 12741–12767.
34 P. Zhai, L. Liu, X. Gu, T. Wang and Y. Gong, *Adv. Energy Mater.*, 2020, **10**, 2001257.
35 L. Qiao, S. R. Peña, M. Martínez-Ibañez, A. Santiago, I. Aldalur, E. Lobato, E. Sanchez-Diez, Y. Zhang, H. Manzano, H. Zhu, M. Forsyth, M. Armand, J. Carrasco and H. Zhang, *J. Am. Chem. Soc.*, 2022, **144**, 9806–9816.
36 P. Zhao, Y. Feng, T. Li, B. Li, L. Hu, K. Sun, C. Bao, S. Xiong, A. Matic and J. Song, *Energy Storage Mater.*, 2020, **33**, 158–163.
37 J. H. Um, K. Kim, J. Park, Y.-E. Sung and S.-H. Yu, *J. Mater. Chem. A*, 2020, **8**, 13874–13895.
38 Z. Zhao, W. Chen, S. Impeng, M. Li, R. Wang, Y. Liu, L. Zhang, L. Dong, J. Unruangsri, C. Peng, C. Wang,

S. Namuangruk, S.-Y. Lee, Y. Wang, H. Lu and J. Guo, *J. Mater. Chem. A*, 2020, **8**, 3459–3467.
39 G. Wang, C. Chen, Y. Chen, X. Kang, C. Yang, F. Wang, Y. Liu and X. Xiong, *Angew. Chem., Int. Ed.*, 2020, **59**, 2055–2060.
40 D. Li, H. Hu, B. Chen and W.-Y. Lai, *Small*, 2022, **18**, 2200010.
41 J. Zhou, M. Xie, F. Wu, Y. Mei, Y. Hao, L. Li and R. Chen, *Adv. Mater.*, 2022, **34**, 2106897.
42 Z. Gao, Q. Liu, G. Zhao, Y. Sun and H. Guo, *J. Mater. Chem. A*, 2022, **10**, 7497–7516.
43 R. Zhao, Y. Wu, Z. Liang, L. Gao, W. Xia, Y. Zhao and R. Zou, *Energy Environ. Sci.*, 2020, **13**, 2386–2403.
44 Z. Li, J. Fu, X. Zhou, S. Gui, L. Wei, H. Yang, H. Li and X. Guo, *Adv. Sci.*, 2023, **10**, 2201718.
45 X. Xie, Z. Wang, S. He, K. Chen, Q. Huang, P. Zhang, S.-M. Hao, J. Wang and W. Zhou, *Angew. Chem., Int. Ed.*, 2023, **62**, e202218229.
46 Z. Gao, Q. Liu, G. Zhao, Y. Sun and H. Guo, *J. Mater. Chem. A*, 2022, **10**, 7497–7516.
47 Y. Y. Hu, R. X. Han, L. Mei, J. L. Liu, J. C. Sun, K. Yang and J. W. Zhao, *Mater. Today Energy*, 2021, **19**, 100608.
48 J. Moon, D. O. Kim, L. Bekaert, M. Song, J. Chung, D. Lee, A. Hubin and J. Lim, *Nat. Commun.*, 2022, **13**, 4538.
49 J.-G. Zhang, W. Xu, J. Xiao, X. Cao and J. Liu, *Chem. Rev.*, 2020, **120**, 13312–13348.
50 W. Liu, P. Liu and D. Mitlin, *Adv. Energy Mater.*, 2020, **10**, 2002297.
51 X. Guan, A. Wang, S. Liu, G. Li, F. Liang, Y.-W. Yang, X. Liu and J. Luo, *Small*, 2018, **14**, 1801423.
52 F. Sun, D. Zhou, X. He, M. Osenberg, K. Dong, L. Chen, S. Mei, A. Hilger, H. Markötter, Y. Lu, S. Dong, S. Marathe, C. Rau, X. Hou, J. Li, M. C. Stan, M. Winter, R. Dominko and I. Manke, *ACS Energy Lett.*, 2020, **5**, 152–161.
53 C. Fang, J. Li, M. Zhang, Y. Zhang, F. Yang, J. Z. Lee, M.-H. Lee, J. Alvarado, M. A. Schroeder, Y. Yang, B. Lu, N. Williams, M. Ceja, L. Yang, M. Cai, J. Gu, K. Xu, X. Wang and Y. S. Meng, *Nature*, 2019, **572**, 511–515.
54 T. Kim, W. Song, D.-Y. Son, L. K. Ono and Y. Qi, *J. Mater. Chem. A*, 2019, **7**, 2942–2964.
55 H. Jia, Z. Wang, B. Tawiah, Y. Wang, C.-Y. Chan, B. Fei and F. Pan, *Nano Energy*, 2020, **70**, 104523.
56 W. Guo, Q. Han, J. Jiao, W. Wu, X. Zhu, Z. Chen and Y. Zhao, *Angew. Chem., Int. Ed.*, 2021, **60**, 7267–7274.
57 D. Yuan, J. Zhao, H. Ren, Y. Chen, R. Chua, E. T. J. Jie, Y. Cai, E. Edison, W. Manalastas, M. W. Wong and M. Srinivasan, *Angew. Chem., Int. Ed.*, 2021, **60**, 7213–7219.
58 L. Ma, J. Cui, S. Yao, X. Liu, Y. Luo, X. Shen and J.-K. Kim, *Energy Storage Mater.*, 2020, **27**, 522–554.
59 K. Lim, J. Popovic and J. Maier, *J. Mater. Chem. A*, 2023, **11**, 5725–5733.
60 Z. Lin, X. Guo, Z. Wang, B. Wang, S. He, L. A. O'Dell, J. Huang, H. Li, H. Yu and L. Chen, *Nano Energy*, 2020, **73**, 104786.
61 S. Zhang, S. Li and Y. Lu, *eScience*, 2021, **1**, 163–177.
62 D. Zhu, G. Xu, M. Barnes, Y. Li, C.-P. Tseng, Z. Zhang, J.-J. Zhang, Y. Zhu, S. Khalil, M. M. Rahman, R. Verduzco and P. M. Ajayan, *Adv. Funct. Mater.*, 2021, **31**, 2100505.
63 W. Zhang, S. Zhang, L. Fan, L. Gao, X. Kong, S. Li, J. Li, X. Hong and Y. Lu, *ACS Energy Lett.*, 2019, **4**, 644–650.
64 T. Hosaka, T. Fukabori, T. Matsuyama, R. Tatara, K. Kubota and S. Komaba, *ACS Energy Lett.*, 2021, **6**, 3643–3649.
65 S. Guo, L. Qin, T. Zhang, M. Zhou, J. Zhou, G. Fang and S. Liang, *Energy Storage Mater.*, 2021, **34**, 545–562.
66 G. Li, S. Liu, Z. Liu and Y. Zhao, *Small*, 2021, **17**, 2102196.
67 D. Kang, S. Sardar, R. Zhang, H. Noam, J. Chen, L. Ma, W. Liang, C. Shi and J. P. Lemmon, *Energy Storage Mater.*, 2020, **27**, 69–77.
68 Q. Chen, W. Zhuang, Z. Hou, Y. Jiang, J. Wan, T. Zhang, Y. Zhao and L. Huang, *Adv. Funct. Mater.*, 2022, **33**, 2210206.
69 Q. Zhao, P. Chen, S. Li, X. Liu and L. A. Archer, *J. Mater. Chem. A*, 2019, **7**, 7823–7830.
70 F. Li, J. He, J. Liu, M. Wu, Y. Hou, H. Wang, S. Qi, Q. Liu, J. Hu and J. Ma, *Angew. Chem., Int. Ed.*, 2021, **60**, 6600–6608.
71 M. Zhu, G. Wang, X. Liu, B. Guo, G. Xu, Z. Huang, M. Wu, H.-K. Liu, S.-X. Dou and C. Wu, *Angew. Chem., Int. Ed.*, 2020, **59**, 6596–6600.
72 Y. Qian, S. Hu, X. Zou, Z. Deng, Y. Xu, Z. Cao, Y. Kang, Y. Deng, Q. Shi, K. Xu and Y. Deng, *Energy Storage Mater.*, 2019, **20**, 208–215.
73 E. Markevich, G. Salitra and D. Aurbach, *ACS Energy Lett.*, 2017, **2**, 1337–1345.
74 J. Xu, W. Lv, W. Yang, Y. Jin, Q. Jin, B. Sun, Z. Zhang, T. Wang, L. Zheng, X. Shi, B. Sun and G. Wang, *ACS Nano*, 2022, **16**, 11392–11404.
75 X. Cui, Y. Chu, X. Wang, X. Zhang, Y. Li and Q. Pan, *ACS Appl. Mater. Interfaces*, 2021, **13**, 44983–44990.
76 W. Wang, Z. Yang, Y. Zhang, A. Wang, Y. Zhang, L. Chen, Q. Li and S. Qiao, *Energy Storage Mater.*, 2022, **46**, 374–383.
77 D. Yang, J. Li, F. Yang, J. Li, L. He, H. Zhao, L. Wei, Y. Wang, X. Wang and Y. Wei, *Nano Lett.*, 2021, **21**, 7063–7069.
78 C. Chen, Q. Liang, Z. Chen, W. Zhu, Z. Wang, Y. Li, X. Wu and X. Xiong, *Angew. Chem., Int. Ed.*, 2021, **60**, 26718–26724.
79 D. Chen, P. Liu, L. Zhong, S. Wang, M. Xiao, D. Han, S. Huang and Y. Meng, *Small*, 2021, **17**, 2101496.
80 Z. Li, W. Ji, T.-X. Wang, Y. Zhang, Z. Li, X. Ding, B.-H. Han and W. Feng, *ACS Appl. Mater. Interfaces*, 2021, **13**, 22586–22596.
81 J. Tan, X. Ao, A. Dai, Y. Yuan, H. Zhuo, H. Lu, L. Zhuang, Y. Ke, C. Su, X. Peng, B. Tian and J. Lu, *Energy Storage Mater.*, 2020, **33**, 173–180.
82 Z. Li, R. Yu, S. Weng, Q. Zhang, X. Wang and X. Guo, *Nat. Commun.*, 2023, **14**, 482.
83 G. Zhang, Y. Hong, Y. Nishiyama, S. Bai, S. Kitagawa and S. Horike, *J. Am. Chem. Soc.*, 2019, **141**, 1227–1234.

84 Z. Wang, Y. Zhang, P. Zhang, D. Yan, J. Liu, Y. Chen, Q. Liu, P. Cheng, M. J. Zaworotko and Z. Zhang, *eScience*, 2022, **2**, 311–318.
85 Y. Yang, S. Yao, Z. Liang, Y. Wen, Z. Liu, Y. Wu, J. Liu and M. Zhu, *ACS Energy Lett.*, 2022, **7**, 885–896.
86 C. Li, R. Liu, Y. Xiao, F. Cao and H. Zhang, *Energy Storage Mater.*, 2021, **40**, 439–460.
87 X. Yao, C. Guo, C. Song, M. Lu, Y. Zhang, J. Zhou, H. Ding, Y. Chen, S. Li and Y. Lan, *Adv. Mater.*, 2023, **35**, 2208846.
88 Z. Xie, B. Wang, Z. Yang, X. Yang, X. Yu, G. Xing, Y. Zhang and L. Chen, *Angew. Chem., Int. Ed.*, 2019, **58**, 15742–15746.
89 D. Yuan, Y. Dou, Z. Wu, Y. Tian, K.-H. Ye, Z. Lin, S. X. Dou and S. Zhang, *Chem. Rev.*, 2022, **122**, 957–999.
90 Y. Wu, H. Zhao, Z. Wu, L. Yue, J. Liang, Q. Liu, Y. Luo, S. Gao, S. Lu, G. Chen, X. Shi, B. Zhong, X. Guo and X. Sun, *Energy Storage Mater.*, 2021, **34**, 483–507.
91 C. Zheng, Y. Yao, X. Rui, Y. Feng, D. Yang, H. Pan and Y. Yu, *Adv. Mater.*, 2022, **34**, 2204988.
92 Y. Qin, H. Li, C. Han, F. Mo and X. Wang, *Adv. Mater.*, 2022, **34**, 2207118.
93 Z. Chang, H. Yang, X. Zhu, P. He and H. Zhou, *Nat. Commun.*, 2022, **13**, 1510.
94 J. Qian, Y. Li, M. Zhang, R. Luo, F. Wang, Y. Ye, Y. Xing, W. Li, W. Qu, L. Wang, L. Li, Y. Li, F. Wu and R. Chen, *Nano Energy*, 2019, **60**, 866–874.
95 X. Wang, X. Chi, M. Li, D. Guan, C. Miao and J. Xu, *Adv. Funct. Mater.*, 2022, **32**, 2113235.
96 F. Zhao, P. Zhai, Y. Wei, Z. Yang, Q. Chen, J. Zuo, X. Gu and Y. Gong, *Adv. Sci.*, 2022, **9**, 2103930.
97 T. Jiang, K. Chen, J. Wang, Z. Hu, G. Wang, X.-D. Chen, P. Sun, Q. Zhang, C. Yan and L. Zhang, *J. Mater. Chem. A*, 2019, **7**, 27535–27546.
98 Z. Wang, H. Chen, H. Wang, W. Huang, H. Li and F. Pan, *ACS Energy Lett.*, 2022, **7**, 4168–4176.
99 J. Meng, H. Zhu, Z. Xiao, X. Zhang, C. Niu, Y. Liu, G. Jiang, X. Wang, F. Qiao, X. Hong, F. Liu, Q. Pang and L. Mai, *ACS Nano*, 2022, **16**, 7291–7300.
100 Y. Fang, R. Lian, H. Li, Y. Zhang, Z. Gong, K. Zhu, K. Ye, J. Yan, G. Wang, Y. Gao, Y. Wei and D. Cao, *ACS Nano*, 2020, **14**, 8744–8753.
101 J. Zheng, Z. Huang, F. Ming, Y. Zeng, B. Wei, Q. Jiang, Z. Qi, Z. Wang and H. Liang, *Small*, 2022, **18**, 2200006.
102 Q. Zhao, S. Stalin and L. A. Archer, *Joule*, 2021, **5**, 1119–1142.
103 S. Kim, G. Park, S. J. Lee, S. Seo, K. Ryu, C. H. Kim and J. W. Choi, *Adv. Mater.*, 2023, DOI: **10.1002/adma.202206625**.
104 E. Peled, *J. Electrochem. Soc.*, 1979, **126**, 2047–2051.
105 L. Guo, F. Huang, M. Cai, J. Zhang, G. Ma and S. Xu, *ACS Appl. Mater. Interfaces*, 2021, **13**, 32886–32893.
106 K. J. Kim, M. Balaish, M. Wadaguchi, L. Kong and J. L. M. Rupp, *Adv. Energy Mater.*, 2021, **11**, 2002689.
107 P. Zhao, Y. Feng, T. Li, B. Li, L. Hu, K. Sun, C. Bao, S. Xiong, A. Matic and J. Song, *Energy Storage Mater.*, 2020, **33**, 158–163.
108 Q. Wang, J. Yang, X. Huang, Z. Zhai, J. Tang, J. You, C. Shi, W. Li, P. Dai, W. Zheng, L. Huang and S. Sun, *Adv. Energy Mater.*, 2022, **12**, 2103972.
109 S.-Y. Lee, J. Shangguan, J. Alvarado, S. Betzler, S. J. Harris, M. M. Doeff and H. Zheng, *Energy Environ. Sci.*, 2020, **13**, 1832–1842.
110 S. Bai, Y. Sun, J. Yi, Y. He, Y. Qiao and H. Zhou, *Joule*, 2018, **2**, 2117–2132.
111 Q. Wu, Y. Zheng, X. Guan, J. Xu, F. Cao and C. Li, *Adv. Funct. Mater.*, 2021, **31**, 2101034.
112 S.-D. Seo, C. Choi, D. Park, D.-Y. Lee, S. Park and D.-W. Kim, *Chem. Eng. J.*, 2020, **400**, 125959.
113 J. Qian, Y. Li, M. Zhang, R. Luo, F. Wang, Y. Ye, Y. Xing, W. Li, W. Qu, L. Wang, L. Li, Y. Li, F. Wu and R. Chen, *Nano Energy*, 2019, **60**, 866–874.
114 J. He, A. Bhargav and A. Manthiram, *Angew. Chem., Int. Ed.*, 2022, **61**, e202116586.
115 Z. Zhao, W. Chen, S. Impeng, M. Li, R. Wang, Y. Liu, L. Zhang, L. Dong, J. Unruangsri, C. Peng, C. Wang, S. Namuangruk, S.-Y. Lee, Y. Wang, H. Lu and J. Guo, *J. Mater. Chem. A*, 2020, **8**, 3459–3467.
116 Z. Li, W. Ji, T.-X. Wang, Y. Zhang, Z. Li, X. Ding, B.-H. Han and W. Feng, *ACS Appl. Mater. Interfaces*, 2021, **13**, 22586–22596.
117 W. Wang, Z. Yang, Y. Zhang, A. Wang, Y. Zhang, L. Chen, Q. Li and S. Qiao, *Energy Storage Mater.*, 2022, **46**, 374–383.
118 D. Chen, S. Huang, L. Zhong, S. Wang, M. Xiao, D. Han and Y. Meng, *Adv. Funct. Mater.*, 2020, **30**, 1907717.
119 Y. Du, H. Yang, J. M. Whiteley, S. Wan, Y. Jin, S.-H. Lee and W. Zhang, *Angew. Chem., Int. Ed.*, 2016, **55**, 1737–1741.
120 X. Li, Y. Tian, L. Shen, Z. Qu, T. Ma, F. Sun, X. Liu, C. Zhang, J. Shen, X. Li, L. Gao, S. Xiao, T. Liu, Y. Liu and Y. Lu, *Adv. Funct. Mater.*, 2021, **31**, 2009718.
121 W. Zhang, G. Jiang, W. Zou, L. Zhang, S. Li, S. Qi, X. Wang, Z. Cui, H. Song, L. Du and Z. Liang, *J. Power Sources*, 2022, **548**, 232001.
122 J. Dong, X. Han, Y. Liu, H. Li and Y. Cui, *Angew. Chem., Int. Ed.*, 2020, **59**, 13722–13733.
123 S.-W. Ke, Y. Wang, J. Su, K. Liao, S. Lv, X. Song, T. Ma, S. Yuan, Z. Jin and J.-L. Zuo, *J. Am. Chem. Soc.*, 2022, **144**, 8267–8277.
124 J.-Y. Hwang, S.-T. Myung and Y.-K. Sun, *Chem. Soc. Rev.*, 2017, **46**, 3529–3614.
125 Z. Hou, W. Wang, Q. Chen, Y. Yu, X. Zhao, M. Tang, Y. Zheng and Z. Quan, *ACS Appl. Mater. Interfaces*, 2019, **11**, 37693–37700.
126 M. Zhu, Y. Zhang, F. Yu, Z. Huang, Y. Zhang, L. Li, G. Wang, L. Wen, H. K. Liu, S.-X. Dou and C. Wu, *Nano Lett.*, 2021, **21**, 619–627.
127 D. A. Rakov, F. Chen, S. A. Ferdousi, H. Li, T. Pathirana, A. N. Simonov, P. C. Howlett, R. Atkin and M. Forsyth, *Nat. Mater.*, 2020, **19**, 1096–1101.
128 L. Gao, J. Chen, Q. Chen and X. Kong, *Sci. Adv.*, 2022, **8**, eabm4606.

129 Q. Lu, A. Omar, L. Ding, S. Oswald, M. Hantusch, L. Giebeler, K. Nielsch and D. Mikhailova, *J. Mater. Chem. A*, 2021, **9**, 9038–9047.
130 S. Wei, S. Choudhury, J. Xu, P. Nath, Z. Tu and L. A. Archer, *Adv. Mater.*, 2017, **29**, 1605512.
131 H. Wang, C. Wang, E. Matios and W. Li, *Nano Lett.*, 2017, **17**, 6808–6815.
132 M. Gu, A. M. Rao, J. Zhou and B. Lu, *Energy Environ. Sci.*, 2023, **16**, 1166–1175.
133 X. Min, J. Xiao, M. Fang, W. Wang, Y. Zhao, Y. Liu, A. M. Abdelkader, K. Xi, R. V. Kumar and Z. Huang, *Energy Environ. Sci.*, 2021, **14**, 2186–2243.
134 N. Xiao, W. D. McCulloch and Y. Wu, *J. Am. Chem. Soc.*, 2017, **139**, 9475–9478.
135 H. Sun, P. Liang, G. Zhu, W. H. Hung, Y.-Y. Li, H.-C. Tai, C.-L. Huang, J. Li, Y. Meng, M. Angell, C.-A. Wang and H. Dai, *Proc. Natl. Acad. Sci. U. S. A.*, 2020, **117**, 27847–27853.
136 Y. Hu, L. Fan, A. M. Rao, W. Yu, C. Zhuoma, Y. Feng, Z. Qin, J. Zhou and B. Lu, *Natl. Sci. Rev.*, 2022, **9**, nwac134.
137 M. Gao, H. Li, L. Xu, Q. Xue, X. Wang, Y. Bai and C. Wu, *J. Energy Chem.*, 2021, **59**, 666–687.
138 B. Liu, J.-G. Zhang and W. Xu, *Joule*, 2018, **2**, 833–845.
139 Z. Li and A. W. Robertson, *Battery Energy*, 2023, **2**, 20220029.
140 J. Hao, B. Li, X. Li, X. Zeng, S. Zhang, F. Yang, S. Liu, D. Li, C. Wu and Z. Guo, *Adv. Mater.*, 2020, **32**, 2003021.
141 T. Wang, C. Li, X. Xie, B. Lu, Z. He, S. Liang and J. Zhou, *ACS Nano*, 2020, **14**, 16321–16347.
142 Y. Zhang, L. Zhao, Y. Liang, X. Wang and Y. Yao, *eScience*, 2022, **2**, 110–115.
143 H. Li, S. Guo and H. Zhou, *Energy Storage Mater.*, 2023, **56**, 227–257.
144 J. Yin, X. Feng, Z. Gan, Y. Gao, Y. Cheng and X. Xu, *Energy Storage Mater.*, 2023, **54**, 623–640.
145 J. Zheng, D. C. Bock, T. Tang, Q. Zhao, J. Yin, K. R. Tallman, G. Wheeler, X. Liu, Y. Deng, S. Jin, A. C. Marschilok, E. S. Takeuchi, K. J. Takeuchi and L. A. Archer, *Nat. Energy*, 2021, **6**, 398–406.
146 P.-F. Zhang, Z. Wu, S.-J. Zhang, L.-Y. Liu, Y. Tian, Y. Dou, Z. Lin and S. Zhang, *Nano Energy*, 2022, **102**, 107721.
147 H. Yu, Y. Chen, W. Wei, X. Ji and L. Chen, *ACS Nano*, 2022, **16**, 9736–9747.
148 H. Huang, D. Xie, J. Zhao, P. Rao, W. M. Choi, K. Davey and J. Mao, *Adv. Energy Mater.*, 2022, **12**, 2202419.
149 H. Yu, Y. Chen, H. Wang, X. Ni, W. Wei, X. Ji and L. Chen, *Nano Energy*, 2022, **99**, 107426.
150 S. Kim, X. Yang, M. Cho and Y. Lee, *Chem. Eng. J.*, 2022, **427**, 131954.
151 Y. Wang, T. Guo, J. Yin, Z. Tian, Y. Ma, Z. Liu, Y. Zhu and H. N. Alshareef, *Adv. Mater.*, 2022, **34**, 2106937.
152 L. Cao, D. Li, T. Deng, Q. Li and C. Wang, *Angew. Chem., Int. Ed.*, 2020, **59**, 19292–19296.
153 M. Liu, L. Yang, H. Liu, A. Amine, Q. Zhao, Y. Song, J. Yang, K. Wang and F. Pan, *ACS Appl. Mater. Interfaces*, 2019, **11**, 32046–32051.
154 X. Hu, Z. Lin, S. Wang, G. Zhang, S. Lin, T. Huang, R. Chen, L.-H. Chung and J. He, *ACS Appl. Energy Mater.*, 2022, **5**, 3715–3723.
155 K. Wu, X. Shi, F. Yu, H. Liu, Y. Zhang, M. Wu, H.-K. Liu, S.-X. Dou, Y. Wang and C. Wu, *Energy Storage Mater.*, 2022, **51**, 391–399.
156 Z. Liang and C. Ban, *Angew. Chem., Int. Ed.*, 2021, **60**, 11036–11047.
157 Q. Pang, J. Meng, S. Gupta, X. Hong, C. Y. Kwok, J. Zhao, Y. Jin, L. Xu, O. Karahan, Z. Wang, S. Toll, L. Mai, L. F. Nazar, M. Balasubramanian, B. Narayanan and D. R. Sadoway, *Nature*, 2022, **608**, 704–711.
158 M. Jiang, C. Fu, P. Meng, J. Ren, J. Wang, J. Bu, A. Dong, J. Zhang, W. Xiao and B. Sun, *Adv. Mater.*, 2022, **34**, 2102026.
159 C. Xu, T. Diemant, X. Liu and S. Passerini, *Adv. Funct. Mater.*, 2023, DOI: **10.1002/adfm.202214405**.
160 Y. Sun, Y. Wang, L. Jiang, D. Dong, W. Wang, J. Fan and Y.-C. Lu, *Energy Environ. Sci.*, 2023, **16**, 265–274.
161 Y. Yoshida, T. Yamada, Y. Jing, T. Toyao, K. Shimizu and M. Sadakiyo, *J. Am. Chem. Soc.*, 2022, **144**, 8669–8675.
162 J. Long, S. Tan, J. Wang, F. Xiong, L. Cui, Q. An and L. Mai, *Angew. Chem., Int. Ed.*, 2023, DOI: **10.1002/anie.202301934**.
163 S.-B. Son, T. Gao, S. P. Harvey, K. X. Steirer, A. Stokes, A. Norman, C. Wang, A. Cresce, K. Xu and C. Ban, *Nat. Chem.*, 2018, **10**, 532–539.
164 Q. Zhao, M. J. Zachman, W. I. Al Sadat, J. Zheng, L. F. Kourkoutis and L. Archer, *Sci. Adv.*, 2018, **4**, eaau8131.
165 Y. Wang, E. Sahadeo and S. B. Lee, *ACS Appl. Energy Mater.*, 2022, **5**, 2613–2620.
166 Y. Zhang, J. Li, W. Zhao, H. Dou, X. Zhao, Y. Liu, B. Zhang and X. Yang, *Adv. Mater.*, 2022, **34**, 2108114.
167 S. Ye, L. Wang, F. Liu, P. Shi and Y. Yu, *eScience*, 2021, **1**, 75–82.
168 M. Zhu, B. Li, S. Li, Z. Du, Y. Gong and S. Yang, *Adv. Energy Mater.*, 2018, **8**, 1703505.
169 J. Zhao, H. Yuan, G. Wang, X. F. Lim, H. Ye, V. Wee, Y. Fang, J. Y. Lee and D. Zhao, *J. Mater. Chem. A*, 2021, **9**, 12099–12108.
170 D. Guo, F. Ming, D. B. Shinde, L. Cao, G. Huang, C. Li, Z. Li, Y. Yuan, M. N. Hedhili, H. N. Alshareef and Z. Lai, *Adv. Funct. Mater.*, 2021, **31**, 2101194.
171 X. Tang, D. Zhou, P. Li, X. Guo, B. Sun, H. Liu, K. Yan, Y. Gogotsi and G. Wang, *Adv. Mater.*, 2020, **32**, 1906739.
172 L. Zhang, S. Peng, Y. Ding, X. Guo, Y. Qian, H. Celio, G. He and G. Yu, *Energy Environ. Sci.*, 2019, **12**, 1989–1998.
173 J. Wang, M. Chen, Z. Lu, Z. Chen and L. Si, *Adv. Sci.*, 2022, **9**, 2203058.
174 Y. Zeng, X. Zhang, R. Qin, X. Liu, P. Fang, D. Zheng, Y. Tong and X. Lu, *Adv. Mater.*, 2019, **31**, 1903675.
175 Q. Wang, L. Jiang, Y. Yu and J. Sun, *Nano Energy*, 2019, **55**, 93–114.
176 Z. Wei, R. Maile, L. M. Riegger, M. Rohnke, K. Müller-Buschbaum and J. Janek, *Batteries Supercaps*, 2022, **5**, e202200318.

177 B. Tang, Y. Zhao, Z. Wang, S. Chen, Y. Wu, Y. Tseng, L. Li, Y. Guo, Z. Zhou and S.-H. Bo, *eScience*, 2021, **1**, 194–202.
178 R. Wang, S. Jeong, H. Ham, J. Kim, H. Lee, C. Y. Son and M. J. Park, *Adv. Mater.*, 2022, **35**, 2203413.
179 S. Xin, Y. You, S. Wang, H.-C. Gao, Y.-X. Yin and Y.-G. Guo, *ACS Energy Lett.*, 2017, **2**, 1385–1394.
180 Y. Lu, L. Li, Q. Zhang, Z. Niu and J. Chen, *Joule*, 2018, **2**, 1747–1770.
181 A. Manthiram, X. Yu and S. Wang, *Nat. Rev. Mater.*, 2017, **2**, 16103.
182 X. Yu, N. S. Grundish, J. B. Goodenough and A. Manthiram, *ACS Appl. Mater. Interfaces*, 2021, **13**, 24662–24669.
183 J. Xu, J. Li, Y. Li, M. Yang, L. Chen, H. Li and F. Wu, *Adv. Mater.*, 2022, **34**, 2203281.
184 Y. Hu, X. Xie, W. Li, Q. Huang, H. Huang, S.-M. Hao, L.-Z. Fan and W. Zhou, *ACS Sustainable Chem. Eng.*, 2023, **11**, 1253–1277.
185 Z. Ye, Y. Jiang, L. Li, F. Wu and R. Chen, *Nano-Micro Lett.*, 2021, **13**, 203.
186 D. Guo, D. B. Shinde, W. Shin, E. Abou-Hamad, A. Emwas, Z. Lai and A. Manthiram, *Adv. Mater.*, 2022, **34**, 2201410.
187 Y. Su, X. Rong, A. Gao, Y. Liu, J. Li, M. Mao, X. Qi, G. Chai, Q. Zhang, L. Suo, L. Gu, H. Li, X. Huang, L. Chen, B. Liu and Y.-S. Hu, *Nat. Commun.*, 2022, **13**, 4181.
188 Y. Wang, S. Geng, G. Yan, X. Liu, X. Zhang, Y. Feng, J. Shi and X. Qu, *ACS Appl. Energy Mater.*, 2022, **5**, 2495–2504.
189 C. Niu, W. Luo, C. Dai, C. Yu and Y. Xu, *Angew. Chem., Int. Ed.*, 2021, **60**, 24915–24923.
190 X. Li, Q. Hou, W. Huang, H.-S. Xu, X. Wang, W. Yu, R. Li, K. Zhang, L. Wang, Z. Chen, K. Xie and K. P. Loh, *ACS Energy Lett.*, 2020, **5**, 3498–3506.
191 Y. Sun, G. Zhao, Y. Fu, Y. Yang, C. Zhang, Q. An and H. Guo, 2022, *Research*, DOI: **10.34133/2022/9798582**.
192 X.-X. Wang, X.-W. Chi, M.-L. Li, D.-H. Guan, C.-L. Miao and J.-J. Xu, *Chem*, 2023, **9**, 394–410.
193 H. Fei, Y. Liu, C. Wei, Y. Zhang, J. Feng, C. Chen and H. Yu, *Acta Phys. – Chim. Sin.*, 2020, **36**, 1905015.
194 Y. Zhou, Z. Xiao, D. Han, L. Yang, J. Zhang, W. Tang, C. Shu, C. Peng and D. Zhou, *Adv. Funct. Mater.*, 2022, **32**, 2111314.
195 X. Wang, C. Zhang, M. Sawczyk, J. Sun, Q. Yuan, F. Chen, T. C. Mendes, P. C. Howlett, C. Fu, Y. Wang, X. Tan, D. J. Searles, P. Král, C. J. Hawker, A. K. Whittaker and M. Forsyth, *Nat. Mater.*, 2022, **21**, 1057–1065.
196 G. Zhao, L. Xu, J. Jiang, Z. Mei, Q. An, P. Lv, X. Yang, H. Guo and X. Sun, *Nano Energy*, 2022, **92**, 106756.
197 S. Park, I. Kristanto, G. Y. Jung, D. B. Ahn, K. Jeong, S. K. Kwak and S.-Y. Lee, *Chem. Sci.*, 2020, **11**, 11692–11698.
198 X. Xu, Y. Xu, J. Zhang, Y. Zhong, Z. Li, H. Qiu, H. B. Wu, J. Wang, X. Wang, C. Gu and J. Tu, *Nano-Micro Lett.*, 2023, **15**, 56.
199 K. Leng, G. Li, J. Guo, X. Zhang, A. Wang, X. Liu and J. Luo, *Adv. Funct. Mater.*, 2020, **30**, 2001317.
200 Z. Chen, X. Li, D. Wang, Q. Yang, L. Ma, Z. Huang, G. Liang, A. Chen, Y. Guo, B. Dong, X. Huang, C. Yang and C. Zhi, *Energy Environ. Sci.*, 2021, **14**, 3492–3501.
201 J. Feng, D. Ma, K. Ouyang, M. Yang, Y. Wang, J. Qiu, T. Chen, J. Zhao, B. Yong, Y. Xie, H. Mi, L. Sun, C. He and P. Zhang, *Adv. Funct. Mater.*, 2022, **32**, 2207909.
202 S. S. Shinde, J. Y. Jung, N. K. Wagh, C. H. Lee, D.-H. Kim, S.-H. Kim, S. U. Lee and J.-H. Lee, *Nat. Energy*, 2021, **6**, 592–604.
203 J. Zheng, D. C. Bock, T. Tang, Q. Zhao, J. Yin, K. R. Tallman, G. Wheeler, X. Liu, Y. Deng, S. Jin, A. C. Marschilok, E. S. Takeuchi, K. J. Takeuchi and L. A. Archer, *Nat. Energy*, 2021, **6**, 398–406.
204 X. Ge, F. Song, A. Du, Y. Zhang, B. Xie, L. Huang, J. Zhao, S. Dong, X. Zhou and G. Cui, *Adv. Energy Mater.*, 2022, **12**, 2201464.
205 Q. Zhao, P. Wu, D. Sun, H. Wang and Y. Tang, *Chem. Commun.*, 2022, **58**, 3282–3285.
206 P. G. Bruce, S. A. Freunberger, L. J. Hardwick and J.-M. Tarascon, *Nat. Mater.*, 2012, **11**, 19–29.
207 A. Manthiram, Y. Fu, S.-H. Chung, C. Zu and Y.-S. Su, *Chem. Rev.*, 2014, **114**, 11751–11787.
208 Z. W. Seh, Y. Sun, Q. Zhang and Y. Cui, *Chem. Soc. Rev.*, 2016, **45**, 5605–5634.
209 H. Zhang, W. Zhao, M. Zou, Y. Wang, Y. Chen, L. Xu, H. Wu and A. Cao, *Adv. Energy Mater.*, 2018, **8**, 1800013.
210 J. Liu, H. Li, J. Wang, Y. Zhang, D. Luo, Y. Zhao, Y. Li, A. Yu, X. Wang and Z. Chen, *Adv. Energy Mater.*, 2021, **11**, 2101926.
211 C. Wei, Y. Wang, Y. Zhang, L. Tan, Y. Qian, Y. Tao, S. Xiong and J. Feng, *Nano Res.*, 2021, **14**, 3576–3584.
212 F. Xu, S. Yang, X. Chen, Q. Liu, H. Li, H. Wang, B. Wei and D. Jiang, *Chem. Sci.*, 2019, **10**, 6001–6006.
213 C. Ye, Y. Jiao, D. Chao, T. Ling, J. Shan, B. Zhang, Q. Gu, K. Davey, H. Wang and S.-Z. Qiao, *Adv. Mater.*, 2020, **32**, 1907557.
214 Z. Huang, B. Song, H. Zhang, F. Feng, W. Zhang, K. Lu and Q. Chen, *Adv. Funct. Mater.*, 2021, **31**, 2100666.
215 S. Bai, X. Liu, K. Zhu, S. Wu and H. Zhou, *Nat. Energy*, 2016, **1**, 16094.
216 S. Bai, B. Kim, C. Kim, O. Tamwattana, H. Park, J. Kim, D. Lee and K. Kang, *Nat. Nanotechnol.*, 2021, **16**, 77–84.
217 Z. Hao, Y. Wu, Q. Zhao, J. Tang, Q. Zhang, X. Ke, J. Liu, Y. Jin and H. Wang, *Adv. Funct. Mater.*, 2021, **31**, 2102938.
218 B. Hu, J. Xu, Z. Fan, C. Xu, S. Han, J. Zhang, L. Ma, B. Ding, Z. Zhuang, Q. Kang and X. Zhang, *Adv. Energy Mater.*, 2023, **13**, 2203540.
219 Y. Yang, S. Yao, Z. Liang, Y. Wen, Z. Liu, Y. Wu, J. Liu and M. Zhu, *ACS Energy Lett.*, 2022, **7**, 885–896.
220 C. Yin, Z. Li, D. Zhao, J. Yang, Y. Zhang, Y. Du and Y. Wang, *ACS Nano*, 2022, **16**, 14178–14187.
221 Z. Deller, L. A. Jones and S. Maniam, *Green Chem.*, 2021, **23**, 4955–4979.

222 F. Zhang, M. Yang, M. Ding and C. Jia, *Front. Chem.*, 2020, **8**, 451.
223 X. Wei, W. Pan, W. Duan, A. Hollas, Z. Yang, B. Li, Z. Nie, J. Liu, D. Reed, W. Wang and V. Sprenkle, *ACS Energy Lett.*, 2017, **2**, 2187–2204.
224 X. Zu, L. Zhang, Y. Qian, C. Zhang and G. Yu, *Angew. Chem., Int. Ed.*, 2020, **59**, 22163–22170.
225 A. Hollas, X. Wei, V. Murugesan, Z. Nie, B. Li, D. Reed, J. Liu, V. Sprenkle and W. Wang, *Nat. Energy*, 2018, **3**, 508–514.
226 S. Huang, H. Zhang, M. Salla, J. Zhuang, Y. Zhi, X. Wang and Q. Wang, *Nat. Commun.*, 2022, **13**, 4746.
227 P. Albertus, S. Babinec, S. Litzelman and A. Newman, *Nat. Energy*, 2018, **3**, 16–21.